DEVELOPMENT OF RADAR-BASED VITAL SIGN DETECTION AND INDOOR TARGET LOCALIZATION ALGORITHMS

LIN WAN
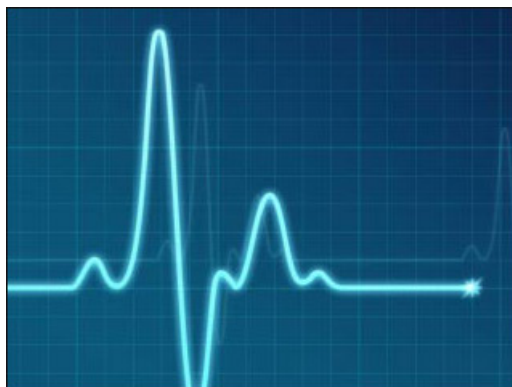
DEVELOPMENT OF RADAR-BASED VITAL SIGN DETECTION AND INDOOR TARGET LOCALIZATION ALGORITHMS

to obtain the degree of Master of Science
in Electrical Engineering
at Delft University of Technology,
to be defended publicly on Friday August 28, 2020 at 09:30 AM

by

LIN WAN

born in Jiangsu, China.

This thesis has been approved by the

      supervisor: Prof. DSc. Alexander Yarovoy
      daily supervisor: Dr. Francesco Fioranelli
      company supervisor: Dr. Marco Mercuri
Thesis committee:

Prof. DSc. Alexander Yarovoy,	MS3 TU Delft
Dr. Francesco Fioranelli,	MS3 TU Delft
Dr. Marco Mercuri,	IMEC Holst centre
Dr. Carolina Varon,	CAS TU Delft

ABSTRACT

In the last two decades, radar-based contactless vital signs monitoring (heartbeat and respiration rate) has raised increasing interest as an emerging approach for healthcare and complementary for other more established technologies. Heartbeat and respiration induce only very subtle rhythmic changes in the reflected radar signature, whereas the signals reflected by larger objects in real scenarios and even the movements of body parts of the subjects being monitored are typically larger. Radar reflection paths are multiple and often vary strongly, especially indoors. It is therefore extremely challenging to determine the correct number of targets and to perform concurrent localization and reliable vital signs monitoring on multiple people in real-world environments. The multipaths (ghost signals) from the reflected signal of one individual, combine with the reflected signals and multipaths of other subjects and with clutter, jeopardizing individual vital signs extraction and localization.

The main research activities in this thesis aimed to extend the work of a previous master thesis from SISO (single input single output) radar to a SIMO (single input multiple output) radar framework. The core idea is that the usage of multiple receiver channels that SIMO radar provides can enable an additional degree of freedom (the estimation of the angular position) to distinguish real targets from ghost targets due to multipath, hence improving their rejection and cancellation.

Simulation results are then generated to compare SISO and SIMO frameworks for recognition of the number of subjects in a given environment, for their localisation, and for the estimation of their vital signs. Unfortunately, due to access limitation caused by the COVID-19 pandemic to the offices of IMEC, Eindhoven, where this thesis work was mostly performed, the initially planned experimental validation with SIMO radar was not possible to perform.

PREFACE

Studying in Delft University of Technology in the past two years is the most memorable experience in my life so far. I feel proud of the improvements that I have made both in my study and life. I cannot imagine what my life would be like if I did not get the help from my supervisors, classmates, friends and family.

First of all, I would like to express my gratitude to my thesis supervisor, Prof. Alexander Yarovoy, who provided me the opportunity to do the master thesis in Group MS3. Every monthly meeting with him, he gave me great encouragement and constructive guidance on work and how to work efficiently.

Then, I sincerely appreciate the guidance of my daily supervisor Dr. Francesco Fioranelli, who keeps encouraging and helping me. He is always willing to share his knowledge and experience with me. He always enlightened me on the insight into a scientific question, which makes me clear to the research questions.

I would like to thank my company supervisor Dr. Marco Mercuri sincerely, who gave me the opportunity to work and do my master thesis in the IMEC Holst Centre. Every meeting with him let me learn quite a lot from his creative and critical thinking. Thanks to his support and give me quite a lot of idea for this thesis. I feel very lucky to have a supportive and friendly company supervisor.

Moreover, I would like to thank all people in Group MS3 and all my colleagues in IMEC Holst Centre.

I am particularly grateful to my friends who bring me warmth and a lot positive energy when I feel lonely and frustrated in a foreign country. Last but not least, I deeply appreciate the love from my family, especially my parents, who unconditionally support me to to pursue my dreams studying far away from hometown.

Lin Wan
Eindhoven, August 2020

Contents

LIST OF FIGURES

LIST OF TABLES

1

INTRODUCTION

Radar technologies have been intensively investigated as an emerging key tool in health care, from which not only the elderly population and their families, caregivers, clinicians, but also economy and society can obtain several benefits (e.g. reducing hospitalisation, more timely and personalised individual care, maintaining quality of life for longer even in case of multiple non-communicable diseases). A lot of research interest areis focused on multi-people contactless (hence non-invasive, or less invasive) vital signs monitoring, specifically the remote sensing of the heartbeat and respiration rate [1–3].

1.1. BACKGROUND

In the last two decades, radar technologies have been investigated as one of the promising measurements for long-term health monitoring, and in particular for remote people localization and vital sign monitoring (i.e. respiratory and heartbeat). The radar sensor systems can operate at a distance, without any explicit user involvement and detect the vital signs non-invasively.

Table 1.1 shows a comparison among contactless vital signs detection approaches and technologies [2]. Compared to other existing vital sign sensing techniques, radar sensor systems have the advantages of not recording images of the subjects or private environments, and not requiring the users to wear, carry or interact with additional devices. Non-invasive vital signs monitoring is mainly based on the periodic motion of the chest due to cardiopulmonary activity. The first vital sign system was introduced by Caro et.al. in the 1970s [4]. After that, many researchers tried to improve the accuracy of vital sign monitoring, the reliability of the radar system, processing speed for real-time monitoring, and power requirements from the hardware structures and signal processing techniques.

1.2. PROBLEM STATEMENT

The goal of this thesis is to explore radar-based approaches to localize multiple subjects in an indoor environment correctly, and to monitor their vital signs accurately.

Approach	Measured vital sign	Main advantage	Main disadvantage
Camera	Respiration heartbeat	Unobtrusiveness	Lighting condition dependent
Infrared	Body temperature	Accuracy	Environment dependent
Visible light	Respiration heartbeat	Low-cost	Lighting condition dependent
Microphone	Respiration heartbeat	Low-cost	Sensitivity to noise
Sonar	Respiration	Environment independent	Insensitivity to small motion
Radar	Respiration heartbeat	Environment independent	Sensitivity to interference

Table 1.1: Contactless vital signs detection approaches and technologies, with quick summary of advantages and disadvantages

However, breathing and heartbeats are very small movements, and they can be easily masked by stronger signals and clutter from any other source in the environment. Heartbeat and respiration induce only very subtle rhythmic changes in the reflected radar signature, whereas real-world environments are highly dynamic and rich of larger moving targets, including body parts of the subjects to be monitored themselves.

Furthermore, propagation paths for the radar signals are multiple and often vary strongly, especially indoors where they can be reflected by walls, ceiling, floor, and objects such as large pieces of furniture. It is therefore extremely challenging to determine the correct number of targets in a given environment, and then perform concurrent localization and reliable vital signs monitoring on multiple people in real-world environments. Essentially, the propagation of the electromagnetic signals between radar and monitored subjects happen over multiple paths, the so-called multipath phenomenon, generating "ghost targets" together with the signature of the real human subjects.

This makes the determination of the real number of subjects in an indoor environment and the consequent estimation of their vital signs a challenging problem, for which definitive algorithms have not been fully developed and validated yet. This thesis aims to formulate and contribute a further step in this research direction.

1.3. Thesis contributions and structure

The main research activities aimed to extend the work of a previous master thesis from SISO (single input single output) radar to a SIMO (single input multiple output) radar framework. The core idea is that the usage of multiple receiver channels that SIMO radar provides can enable an additional degree of freedom (the estimation of the angular position) to distinguish real targets from ghost targets due to multipath, hence improving their rejection and cancellation. Simulation results are then generated to compare SISO

and SIMO frameworks for recognition of the number of subjects in a given environment, for their localisation, and for the estimation of their vital signs. Unfortunately, due to access limitation caused by the COVID-19 pandemic to the offices of IMEC, Eindhoven, where this thesis work was mostly performed, the initially planned experimental validation with SIMO radar was not possible to perform.

The key contributions of this thesis work are summarised in the following bullet points.

- Detailed analysis of the multipath effects for the problem of vital signs indoor estimation, with key assumptions in the developed model.

- Construction and full characterisation of the SIMO radar data cube for further processing in the range-Doppler-angle domain.

- Formulation of angular localisation algorithm as part of vital signs estimation process for multiple subjects in SIMO radar framework.

- New definition of an SNR metric for the estimation of the number of subjects

- Validation and comparison of performances of SISO and SIMO vital sign estimation

The general structure of the following sections of this thesis are summarised below.

- Literature review (section 2)

- FMCW Radar system description and theory (section 3)

- Multipath signals model and removal processing (section 4)

- Formulation of the proposed algorithms (section 5)

- Tests on selected simulation cases (section 6)

- Monte Carlo simulations for generalisation of the proposed approach (section 7)

- Conclusions and future work (section 8)

2

LITERATURE REVIEW

In this section, both the single channel radar and multiple channel radar vital sign monitoring approaches are reviewed.

2.1. SINGLE CHANNEL RADAR VITAL SIGN MONITORING

Single-tone CW radar is the most common type in radar-based vital signs monitoring system due to its simplicity and low power consumption. But it cannot detect the vital signs of multi-subject at the same time since it cannot provide range information.

FMCW and UWB radar are capable of measuring both range and Doppler frequency, therefore they can fulfill the functionality of multi-target detection. However, FMCW radar system suffer from high phase noise level and power consumption.

UWB radar system has been proven to have great penetration ability, giving dominant position for applications of search and rescue. But IR-UWB radar is limited by its power density restriction, leading to short distance applications. Performance of different radar systems for vital signs monitoring is summarized in Table 2.1 [5] [6].

System	Multi-subject detection	Range estimation	Power consumption
CW	No	No	Medium
FMCW	Yes	Yes	High
IR-UWB	Yes	Yes	Low

Table 2.1: Comparison of Radar-Based Vital Signs Monitoring Systems

Low-pass filters, high-pass filters, and complex digital signal processing algorithms [7] have been reported for noise filtering and DC offsets elimination. Filtering at signal processing level, including Finite Impulse Response (FIR) [8] and Infinite Impulse Response (IIR) filters have also been proposed.

Other phase-modulation methods have also been proposed to address DC offset. These include using arctangent demodulation technique with DC offset calibrated through

2

empty-room measurements [9]. However, these methods may not be valid because the DC offset value depends on the surface reflectivity, the size of the stationary portion of the target, and cannot be calibrated other than the subject under test. Complex signal demodulation method using Bessel's functions has also been explored to remove DC offset; however, it is still affected by the even order harmonics that are present in the baseband signal [7].

The main limitation in Doppler radar measurement of periodic motions is the presence of phase-nulling or null-point. The most prevailing solution is the quadrature (I/Q) architecture, where at least one of the outputs I/Q is not at null-point. Channel selection is then required to select the most optimum channel for processing at any given point in time [10]. However, I/Q output channels are not always in quadrature because of the inherent amplitude and phase imbalance due to imperfect system components. The contribution of extra flicker noise caused by the mixers also contribute to the degradation of the detection accuracy [10].

The arctangent demodulation method combines the in-phase and quadrature baseband signals into a single channel to eliminate null-point. The successful arctangent demodulation depends on the correction of channel imbalances and the removal of undesired DC offsets. Channel imbalances can be corrected by using Gram-Schmidt procedure [11], however complex calibrations on the DC offsets is required for accurate demodulation [10].

Empirical Mode Decomposition (EMD) has been noted in the literature as an effective method in analyzing non-stationary and non-linear signals. Its application for non-contact Doppler radar system in separating and removing motions artefacts has also been proposed. As documented in the literature, EMD is used for breaking down the radar signal output into its Intrinsic Mode Functions (IMFs). The removal of the motions artefacts interferences is achieved by selecting the proper IMFs. However, the proposed EMD application has its limitation in handling the interferences that occur at frequencies very close to the heart rate. EMD is also limited in removing interferences of the same type from the background objects [12]

In an attempt to address the multi-targets cancellation problem, a technique referred to as Generalized Likelihood Ratio Test (GLRT), based on a model of the heartbeat was proposed to firstly distinguish between the presence of 2, 1, or 0 subjects using a single-antenna Doppler radar system. Using multiple antennas will also result in detection of up to 2N-1 subjects. The use of a single antenna method is based on the subject's heartbeat signature in the frequency domain, and the use of the multiple antennas method is based on the angle of signal arrival. The results demonstrated the theoretical concept; however, accuracy and reliability were not consistent when this method was applied [13].

The location of the targets are often known by ranging the distance between the targets and antenna. Therefore, the vital sign features are not applied in the localization steps and there will be some problems about the ranging when there are some objects near the targets. In paper [14], the standard derivation (std) method was applied by calculating the std of the phase history. The idea is that the physiological movements, over an interval of time of a few seconds, involve a larger standard deviation than static objects. Therefore, the range bins with large variations indicate the location of human targets. In the student work [8], the optimization method was employed by find the optimal

solution of the cost function of the signal model.

When the sources of noise are cancelled, the approaches of extracting the vital signs can be applied. There are some techniques to obtain and classify the breathing rate/heartbeat from the baseband received signal of the microwave sensor. The fast Fourier transform (FFT) [15][16] and continuous wavelet transform (CWT) [17] [8] are considered as very basic methods to retrieve the respiratory rate. These techniques can find the frequency spectrum of received signals, based on the peak of the spectrum in a specific frequency range, and the breathing rate or heartbeat can be estimated.

2.2. MULTIPLE CHANNELS RADAR VITAL SIGN MONITORING

The radar system with multiple receiving channels, which can be termed as single-input multiple-output (SIMO), is used to achieve further improvement. SIMO radar systems fuse the information from multiple channels to improve the detection performance. Akiyama et al. [18] used a system with one transmitting antenna and four receiving antennas to improve the signal-to-noise ratio (SNR) with correlation processing.

Liu et al. [19] demonstrated that the SIMO radar systems have the ability to resolve multiple sources and obtain the angle-of-arrival (AOA) of multiple human targets. Multiple-input and multiple-output (MIMO) radar is a special type of multiple channels radar which emerged in recent years. The MIMO array with M transmitting elements and N receiving elements can obtain a virtual aperture with M by N virtual transceivers, which greatly reduces the weight and cost of the radar system.

MIMO radar echo data can be decomposed as the data from multiple SIMO radar system , since the MIMO radar system can attain and use information from more sight angles. UWB MIMO radar combines the high range resolution property of the UWB signaling with the directional resolution property of the multiple antenna elements, so it has the ability of two-dimensional high-resolution imaging [20].

In paper [21], UWB MIMO radar is exploited to improve the detection performance of multiple stationary humans for its multiple sight angles. To improve the detection performance of human targets caused by heavy clutters, the constant false alarm rate (CFAR), morphological filtering and clustering is implemented.

Recently, [22] introduced a highly integrated 120 GHz MIMO radar system for 3D localization and simultaneous vital sign detection of human subjects. This MIMO radar has the capability to detect and separate the respiration and heart signal of two human subjects.

The conventional DOA estimation in MIMO radar systems can be categorized into two types: non-parametric (spectral-based) methods and parametric methods. The nonparametric algorithms (Bartlett, Capon, MUSIC and ESPRIT) exploit some spectrum-based function of the parameters to be estimated . The parametric techniques, e.g., Deterministic Maximum Likelihood (DML [23]) algorithms have excellent DOA estimation performance. However, they require accurate initialization to guarantee the convergence of the algorithms and suffer from high computational complexity.

The non-parametric methods include conventional digital beamforming and subspace-based algorithm. Although the subspace-based algorithm (MUSIC and ESPRIT) have very good performance on angular resolution, the main challenge of these super resolution DOA estimation algorithm is strongly correlated or coherent sources, the limited

number of snapshots (sometimes even single snapshot), and the unknown number of targets [24].

In FMCW radar systems, beat signals convey range and angle information, which enables to estimate the azimuth, elevation, range, and velocity of unknown targets via joint parameter estimation techniques such as 2D-MUSIC, 2D-ESPRIT, JADE, and multidimensional Capon. However, such multi-dimensional sub-space techniques increased the computational complexity quite a lot, which needs to be considered in a real-time FMCW automotive radar system [25].

2.3. CONCLUSIONS

In summary, from the analysis of the aforementioned techniques and approaches, it is evident that radar-based monitoring of vital signs of multiple people in an indoor environment is still an outstanding research challenge.

Specifically, one aspect of the challenge is the presence of multipath and the related replicas (ghost targets) of the signatures of real targets; these are often not easily distinguishable from the signature of authentic, different real subjects.

Hence, an interesting research direction is the formulation of algorithms and approaches that can enhance the capability of identifying multipath-related signatures (i.e. ghost targets, replicas of real ones) and then discard them. While this problem was partially approached by a previous master work performed between IMEC and TU Delft [8], in this thesis we aim to further extend the research into a SIMO radar framework, exploring how the angular information estimated from multiple channels can improve performances.

The popular signal processing approaches in vital signs monitoring and angle estimation approaches are summarized in Table 2.2 which will be used for vital sign phase extraction and frequnecy estimation and angluar estimation of the targets.

Approach	Reference	Main functions
Phase unwrap	[9]	phase extraction
Linear demodulation	[1]	phase extraction
Wavelet decomposition	[17] [8]	Signal decomposition
EMD	[12]	Signal decomposition
Digital beamforming	[18]	Angle estimation
1D MUSIC	[23]	Angle estimation

Table 2.2: Signal processing approaches in vital signs monitoring and angle estimation

3

FMCW RADAR SYSTEM MODEL

The ideal non-contact health monitoring system aims to monitor the Respiration Rate (RR) and Heartbeat Rate (HR) of multiple stationary subjects. The electromagnetic waves are sent into the environment by the transmitting antenna and are reflected by all the objects in the room, carrying the range (physical distance) and physiological information. Those reflected signals arrive at the receiving antenna through multiple paths, introducing different time of flights (ToFs) and making the indoor localization and vital sign monitoring more complicated. This section presents a short summary of the model of FMCW radar signal, specifically in the case when this is used for vital signs monitoring.

3.1. THEORY OF FMCW RADAR

The transmitted signal of an FMCW radar system is a sweep signal, whose frequency is linearly modulated in time, as is shown in Figure 3.1. In signal processing, the transmitted chirp signal $s_T(t)$ is usually expressed in complex form,

$$
\begin{aligned}
s_T(t) &= a_T e^{j2\pi \int_0^t \left(f_0 + \frac{Bw}{Tc}t\right)dt} \\
&= a_T e^{j2\pi \left(f_0 + \frac{Bw}{Tc}t\right)t}, 0 < t < T_c
\end{aligned}
\tag{3.1}
$$

a_T is the complex amplitude, indicating the transmitted power and the initial phase, f_0 is the starting frequency, Bw is the bandwidth, and T_c is the sweep period.

The corresponding reflected signal $s_R(t)$ in case of a static target is nothing but generally modelled as a delayed and attenuated copy of the transmitted signal, which can be express by:

$$
\begin{aligned}
s_R(t) &= s_T(t - \tau) \\
&= a_R e^{j2\pi \left(f_0 + \frac{Bw}{Tc}(t-\tau)\right)(t-\tau)}
\end{aligned}
\tag{3.2}
$$

a_R is the complex amplitude, indicating the reflected power and the initial phase, f_0 is the starting frequency, Bw is the bandwidth, and T_c is the sweep period, τ is the propagation delay of a certain path.

9
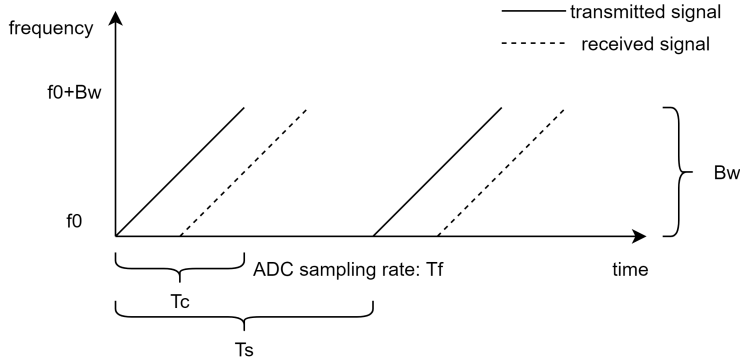
Figure 3.1: Chirp signal in frequency vs time domain

3.2. DOPPLER EFFECT

Figure 3.2 depicts block diagram of range measurement principle FMCW radar system. The shifted reflected signal mixes is mixed with a copy of the transmitted signal stored generated and low-pass filtered, at the Local Oscillator (LO), generating producing a beat-frequency signal $s_B(t)$,

$$
\begin{aligned}
s_B(t) &= a_T e^{j2\pi\left(f_0+\frac{Bw}{Tc}t\right)t} a_R e^{-j2\pi\left(f_0+\frac{Bw}{Tc}(t-\tau)\right)(t-\tau)} \\
&= a_T a_R e^{j2\pi\left(f_0\tau-\frac{Bw}{2Tc}\tau^2+\frac{Bw}{Tc}\tau t\right)} \\
&\approx a_T a_R e^{j2\pi\left(f_0\tau+\frac{Bw}{Tc}\tau t\right)} \\
&= \underbrace{a_T a_R e^{j2\pi f_0\tau}}_{a_B} e^{j2\pi\frac{Bw}{Tc}\tau t} \\
&= a_B e^{j2\pi\frac{Bw}{Tc}\tau t}
\end{aligned}
\tag{3.3}
$$

Here a_B is the complex amplitude of the beat frequency signal and the quadratic term is neglected as it is very small.

From equation 3.3, we can know that the beat frequency signal of each reflected signal is a tone with beat frequency

$$
f_B = \frac{Bw}{Tc}\tau
\tag{3.4}
$$

Which is proportional to the propagation delay . Intuitively, we also can see that the frequency difference between the transmitted signal and the received signal is linearly correlated with propagation delay.

Since the propagation delay is decided by the length of the propagation path

$$
\tau = \frac{2d_0}{c}
\tag{3.5}
$$

here d_0 is the path distance, c is the speed of light. Once we know the beat frequency, which can be easily estimated by performing Fast Fourier Transform (FFT), we know the
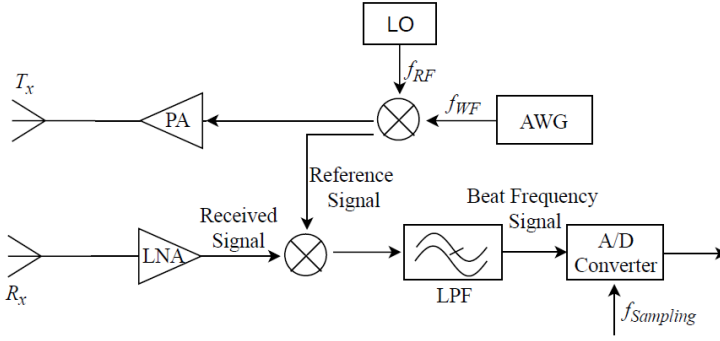
Figure 3.2: Block diagram of FMCW radar principle

path distance

$$d_0 = \frac{\tau c}{2} = \frac{f_B c B w}{2 T_c} \tag{3.6}$$

This is the principle of range measurement in FMCW radar systems.

For human subjects, the beat-frequency signal has a Doppler component because of the physiological motions of chest and abdomen, which introduce some vibrations in range detection. In this case, the propagation delay is not a constant but a function of time, $\tau(t)$. This small variation detected by the radar can be utilized to realize the vital signs monitoring in our system.

The equation that links the Doppler with the velocity of a target, here for the generic/ideal case of the point target is:

$$f_D = \frac{2 v f_c}{c} \tag{3.7}$$

Assume that there are L narrowband signals arriving onto the array and N sensors in the array (Figure 3.3) have identical isotropic responses. The digitized time domain beat signal, which is retrieved after deramping of the transmitted FMCW waveform and under the narrow band assumption, can be modeled as:

$$s(t) = \sum_{l=1}^{L} a_l e^{j2\pi \frac{Bw}{Tc} \tau_l t} e^{j \frac{2\pi}{\lambda} d n \sin\theta_l} \tag{3.8}$$

where a complex amplitude and phase of the l-th target, R, is a range to the l-th target, Bw is the transmitted signal bandwidth, c is the speed of light, T_c is the duration of sweep, λ is the wavelength of the transmitted signal, d is the array elements spacing, , θ is the direction of arrival of signal from the l-th target,

3.3. VITAL SIGN MODEL

Non-contact health monitoring is based on remote sensing of cardiopulmonary activities, heartbeat and respiration. The inhalation and exaltation processes during breath-
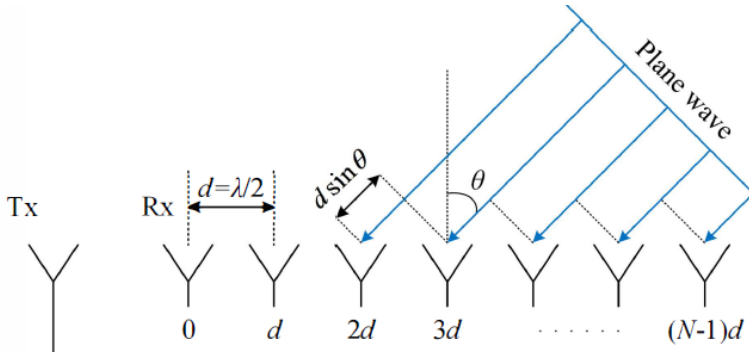
Figure 3.3: Diagram of a uniform linear array for a SIMO radar

ing and the contracting and relaxing of the atria and ventricles when pumping blood through the heart all have contribution to the chest surface motion, which for the radar is a disturbance source in range detection.

More realistic model (rather than sine) of vital signs are possible [26], but for the time being this kind of signal model are not considered here.

Based on the assumption that the chest surface motion is a short-term stationary process, a commonly used parametric model of heartbeat component $R_h(t)$ is a sine wave which is:

$$R_h(t) = \alpha_h \sin\left(2\pi f_h t + \varphi_h\right) \tag{3.9}$$

where α_h and f_h are deterministic, unknown amplitude, angular frequency and φ_h is initial phase of the heartbeat signal.

Similarly, the respiration component $R_r(t)$ can also be modelled in the same way,

$$R_r(t) = \alpha_r \sin\left(2\pi f_r t + \varphi_r\right) \tag{3.10}$$

where α_r and f_r are deterministic, unknown amplitude, angular frequency and φ_r is initial phase of the respiration signal in a short term.

Therefore, the chest surface motion y(t) as the sum of two sine waves,

$$R(t) = R_h(t) + R_r(t) = \alpha_h \sin\left(2\pi f_h t + \varphi_h\right) + \alpha_r \sin\left(2\pi f_r t + \varphi_r\right) \tag{3.11}$$

The typical values of respiration and heartbeat frequency and amplitude are displayed in Table 3.1 [26].

	Frequency[Hz]	Amplitude[mm]
Respiration	0.1-0.4	4-12
Heartbeat	0.83-1.67	0.3-0.6

Table 3.1: Typical frequencies and amplitudes of vital signs

If considering this disturbance in range detection, the corresponding time-varying path distance d(t) and propagation delay $\tau(t)$ are

$$d(t) = d_0 + R(t) \tag{3.12}$$

$$\tau(t) = 2\frac{d_0 + R(t)}{c} \tag{3.13}$$

If we calculate the maximal velocity of the weakest vital sign, we can select the observation time. The maximal velocity of the weakest heart activity is:

$$
\begin{aligned}
v_{h,\min} = \max\left(\frac{dR_h(t)}{dt}\right) &= \max\left(\alpha_{h,\min}2\pi f_{h,\min}\cos\left(2\pi f_{h,\min}t + \varphi_h\right)\right) = \alpha_{h,\min}2\pi f_{h,\min} \\
&= 1.5645[\text{mm/s}]
\end{aligned}
\tag{3.14}
$$

The maximal velocity of the weakest respiration activity is:

$$v_{r,\min} = \max\left(\frac{dR_r(t)}{dt}\right) = \max\left(\alpha_{r,\min}2\pi f_{r,\min}\cos\left(2\pi f_{r,\min}t + \varphi_r\right)\right) = \alpha_{r,\min}2\pi f_{r,\min} = 3.2673\left[\frac{mm}{s}\right] \tag{3.15}$$

The global maximal velocity of the weakest vital signs to be measured is:

$$v_{\min} = \min\left(v_{r,\min}, v_{h,\min}\right) = 1.5645\left[\frac{mm}{s}\right] \tag{3.16}$$

In order to be able to measure the maximal velocity of the weakest chest movement at $f_0 = 7.3$ GHz, the required observation time T_d of the chirp train is:

$$\Delta v = \frac{c}{2T_d f_0} \leq v_{\min} \rightarrow T_d \geq \frac{c}{2v_{\min}f_0} = 13.134[s] \tag{3.17}$$

Therefore, the required measurement time T_d is at least 13.134 s and the coherent processing interval (CPI) of 20s is selected in this work.

3.4. RESOLUTION AND AMBIGUITY

We know that the beat frequency is related to time delay and path distance which is our signal of interest. Assume $w(t) = \delta(t - nT_s)$, where Ts is the fast time sampling interval and n is from 0 to N-1, is a window function (rectangular window). The DTFT of the beat-frequency signal with N samples is

$$
\begin{aligned}
S_B(\omega, t) &= \mathscr{F}\{s_B(t) \cdot w(t)\} \\
&= \mathscr{F}\left\{a_B e^{j2\pi\frac{Bw}{Tc}\tau(t)t} \cdot w(t)\right\}
\end{aligned}
\tag{3.18}
$$

In practice, $S_B(, t)$ is estimated via an FFT whose result is denoted as $S_B(k, t)$, which is a sampled version of DTFT,

$$S_B(k, t) = A(k)e^{j\phi(t)} \tag{3.19}$$

where k is the frequency bin index of FFT, from 0 to N-1.

The disturbance caused by cardiopulmonary activities in range detection is regarded as the vital signs of subjects. And the range is estimated by resolving the beat frequency. However, the resolution of FFT, f, is restricted by the sweep period,

$$\Delta f = \frac{1}{T_c} \tag{3.20}$$

Therefore, the range resolution Δd of a radar system is also limited,

$$\Delta d = \frac{c\Delta f}{2\frac{Bw}{Tc}} = \frac{c}{2Bw} \tag{3.21}$$

Bw is the radar bandwidth. The amplitude of chest surface motion is around 1cm, so the frequency resolution is not sufficient to reflect the chest surface motion. However, the phase of the resulting frequency domain signal $S_B(k, t)$ still preserves the Doppler-Doppler information.

3.5. CONCLUSION

First, the bandwidth using by the IMEC radar is 1GHz which leads to the range resolution to be 0.15 meters. Due to FMCW radar, the vital signs are detected from the phase changes rather than the displacements. So here, the smallest amplitude of the vital sign shown in Table 3.1 are not related to the range resolution. While for the UWB radar, this smallest value which is 0.3mm are related to the range resolution. The vital sign observation time are related to the doppler resolution. The angle resolution is related to the number of sensors. When we let array elements spacing equal to $\lambda/2$, we can get the max angle range from -90 degrees to 90 degrees.

4

MULTIPATH MODEL AND REMOVAL PROCESSING

In this section, the multipath model will be discussed and the corresponding removal processing techniques are also discussed.

4.1. MULTIPATH ANALYSIS AND SIGNAL MODEL ASSUMPTION

In a wireless communication system, multipath interference is always an annoying issue. It occurs when a signal takes two or more paths from the transmitting antenna to the receiving antenna, resulting in ghost subjects and inter-subject interference. It is known that in an indoor environment, the reflected rays arrive at the receiving antenna in clusters. The power gain of different clusters and of rays within a cluster obey the exponential power decay. [8]

While in the radar system, we should also consider the Doppler shift, as in equation 4.1 that shows the multipath model for a radar system

$$h(t) = \sum_{l=1}^{N} \beta_l \cdot \delta\left(t - \tau_l\right) \cdot \delta\left(f - \Delta f_l\right) \tag{4.1}$$

where l is the number of propagation paths, β_l is the amplitude of the reflection, τ_l is the delay of the different paths, Δf_l is the Ddoppler shift of the path.

Figure 4.1 shows an example geometry of the multipath effect for one possible additional path. From the sensor to the wall, the distance is a.

The distance to the ghost target P' is

$$R' = \sqrt{R^2 + 4a^2 - 4aR\sin\left(\theta_1\right)} \tag{4.2}$$

While the angle is

$$\theta_2 = \arctan\left(\frac{2a - R\sin(\theta)}{R\cos(\theta)}\right) \tag{4.3}$$
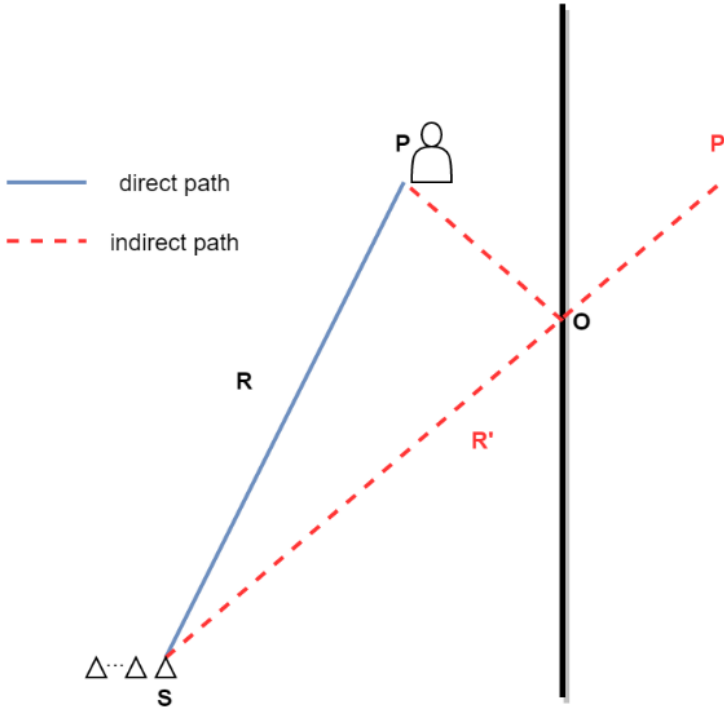
Figure 4.1: Geometry of multipath where 'O' indicates the bouncing point of the EM propagation rays on the wall

The component of the velocity pointing to the reflecting surface is

$$v_r' = v_r \cos(\theta_1 + \theta_2) \tag{4.4}$$

with v_r being the radial component of the velocity of P. Note that the angles are defined with respect to the ordinate.

Apart from the direct path, three ray paths are generally considered as possible sources of multipath.

- First, from the sensor S to the target and backwards over the wall.

- Second, from the sensor to the wall to the target and on the direct path backwards, or alternatively from the sensor to the wall to the target and on the direct path backwards (single bounces)

- third, from the sensor to the wall to the target and the same way back (double bounce)

For the real target this results in a Doppler shift of

$$f_{D,\text{Real}} = \frac{f_0}{c} 2 \overrightarrow{v_r} \cdot \vec{e}_{SP} \tag{4.5}$$

where v_r is the velocity vector of the moving target, c the speed of light, f_0 the transmitted centre frequency, and $\vec{e}_{SP}$ the unit vector from the sensor to the target P.
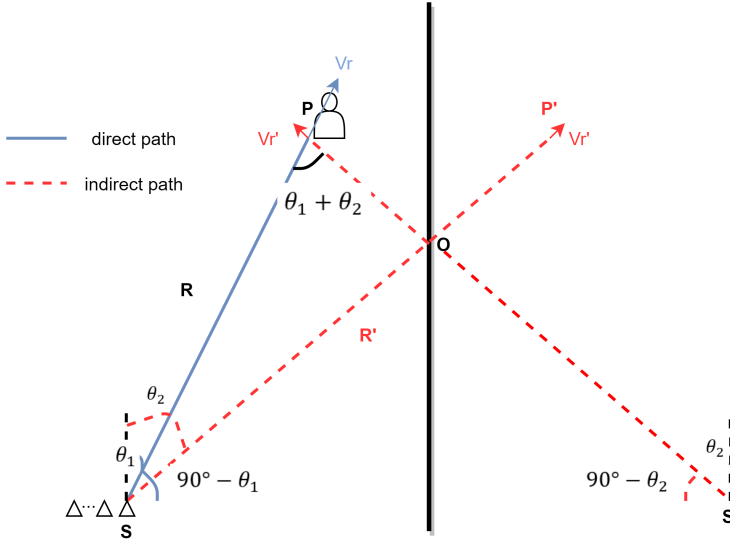
Figure 4.2: Further multipath analysis with propagation paths and angles indicated

For the ghost target, the Doppler shift

$$f_{D,Ghost} = \frac{f_c}{c} 2\overrightarrow{v_r'} \cdot \vec{e}_{SP'} = \frac{f_c}{c} 2\overrightarrow{v_r} \cos(\theta_1 + \theta_2) \vec{e}_{SP'} \tag{4.6}$$

Therefore, the Doppler shift difference between the real target and the ghost target is

$$\Delta f_D = (1 - \cos(\theta_1 + \theta_2)) \frac{f_c}{c} 2\overrightarrow{v_r} \tag{4.7}$$

From the previous calculation of the velocity of the vital sign

$$v_{\min} = \min(v_{r,\min}, v_{h,\min}) = 1.5645 \left[\frac{mm}{s} \right] \tag{4.8}$$

By inserting the v_{min} into the Doppler shift difference, we can get,

$$\Delta f_D \leq 0.0761 \text{Hz} \tag{4.9}$$

If we use the observation time 20s, which means Td=20s, we can get the doppler shift is $1/T_d$ =0.05 Hz. Therefore, with the 0.05Hz resolution, it is difficult to resolve the Doppler shift difference between the real and ghost target.

Figure 4.3 range Doppler plot of raw experimental FMCW SISO data (2 real target and 1 ghost target) From Figure 4.3, the two real targets are in about 1.5 and 2.5 meters and the ghost targets are at about 3.5 meters. We can see it is difficult to resolve the Doppler frequency difference between the real target and the ghost target.
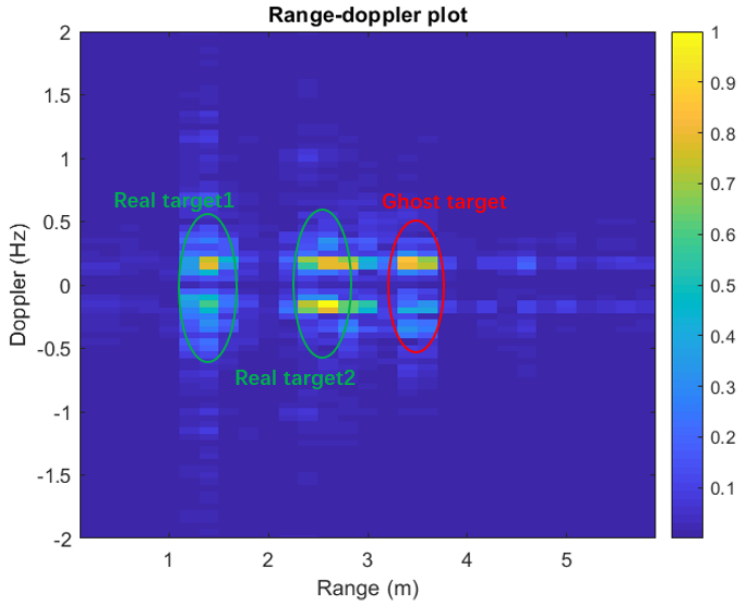
Figure 4.3: range Doppler plot of raw experimental FMCW SISO data (2 real target and 1 ghost target)

With the above analysis of the multipath effect when considering the small Doppler of vital signs and the estimation of the available Doppler resolution for the actual FMCW radar data in this study, we can simplify the multipath propagation model into the following model. Essentially, the Doppler difference between the direct path and the replicas originated by multipath is neglected.

$$h(t) = \sum_{l=1}^{L-1} \beta_l \cdot \delta(t - \tau_l) \qquad (4.10)$$

where l is the number of propagation paths, β_l is the amplitude of the reflection, τ_l is the delay of the different paths

4.2. MULTIPATH ARRAY SIGNAL MODEL FOR FMCW RADAR

It is a generalization of all the possible propagation models that occur in practice. Though it is not a structured one, we can still specify the statistical properties of the model coeffcients at a later stage. Therefore, the received parametric signal model $s_R(t)$ over a multipath channel can be corrected as the convolution

$$s_R(t) = h(t) * s_T(t)$$

$$= \left[\sum_{l=0}^{L-1} \beta_l \delta\left(t - \tau_l(t)\right) \right] * s_T(t)$$

$$= \sum_{l=0}^{L-1} \beta_l s_T\left(t - \tau_l(t)\right)$$

$$= \sum_{l=0}^{L-1} \beta_l \underbrace{a_{T_l} e^{j2\pi\left(f_0 + \frac{\rho}{2}\left(t - \tau_l(t)\right)\right)\left(t - \tau_l(t)\right)}}_{a_{R_l}}$$

$$= \sum_{l=0}^{L-1} a_{R_l} e^{j2\pi\left(f_0 + \frac{\rho}{2}\left(t - \tau_l(t)\right)\right)\left(t - \tau_l(t)\right)}$$

$$(4.11)$$

The corresponding baseband signal model $s_B(t)$ is then

$$s_B(t) = \sum_{l=0}^{L-1} s_R(t) \cdot s_T^{-1}(t)$$

$$= \sum_{l=0}^{L-1} \underbrace{a_T a_R e^{j2\pi f_0 \tau_l(t)}}_{a_{B_l}(t)} e^{j2\pi \cdot \rho \tau_l(t) t}$$

$$= \sum_{l=0}^{L-1} a_{B_l}(t) e^{j2\pi \cdot \rho \tau_l(t) t}$$

$$= \sum_{l=0}^{L-1} s_{B_l}(t)$$

$$(4.12)$$

After performing FFT in fast-time, the frequency domain signal S(k,m) becomes

$$S(k, m) = \mathscr{F}\left\{ \sum_{l=0}^{L-1} s_{B_l}(t) \cdot w(t) \right\} \cdot \delta\left(t - mT_s'\right)$$

$$= \sum_{l=0}^{L-1} \mathscr{F}\left\{ s_{B_l}(t) \cdot w(t) \right\} \cdot \delta\left(t - mT_s'\right)$$

$$= \underbrace{\sum_{l=0}^{L-1} A_l(k) e^{j\phi(m)}}_{A'(k)}$$

$$= A'(k) e^{j\phi(m)}$$

$$(4.13)$$

The aforementioned observation signal S(k,m) is a dual-variable function of frequency index k and discrete slow-time m, forming a 2D observation matrix denoted as X. To explore the characteristics of the observation matrix, it is necessary to do matrix factorization to isolate the signal of interest. Then the observation matrix X including all the samples becomes

$$X = \begin{bmatrix} S(0,0) & \cdots & S(0,M-1) \\ \vdots & \ddots & \vdots \\ S(L-1,0) & \cdots & S(L-1,M-1) \end{bmatrix} : L \times M \tag{4.14}$$
$$= \begin{bmatrix} x_0 & x_1 & \cdots & x_{M-1} \end{bmatrix}$$

It follow that X has a factorization that

$$X = hs \tag{4.15}$$

Where

$$s = \begin{bmatrix} e^{j\phi(0)} & e^{j\phi(1)} & \cdots & e^{j\phi(M-1)} \end{bmatrix} : 1 \times M$$

$$h = \begin{bmatrix} A(0) \\ A(1) \\ \vdots \\ A(L-1) \end{bmatrix} : L \times 1 \tag{4.16}$$

Here s contains the Doppler information due to the physiological activities. Time shifts in propagation delay resulting in frequency and range shifts in range, therefore h contains the attenuation and time delay information of the propagation channel for each reflector. Obviously, X is a rank-1 matrix and it spans the same row space with s. However, this is the data model for single user case, in a real indoor environment, there are a lot of static clutters and what we are interested in is the multi-user case. So this simple model is going to be extended to a more complicated one for more practical applications.

Suppose P targets multiple users case, the S(k,m) will becomes

$$S(k,m) = \sum_{i=1}^{P} A_i(k) e^{j\phi_i(m)} \tag{4.17}$$

Then X has the following factorization

$$X = HS \tag{4.18}$$

Where

$$H = \begin{bmatrix} A_1(0) & \vdots & A_P(0) \\ A_1(1) & \vdots & A_P(1) \\ \vdots & \vdots & \vdots \\ A_1(L-1) & \vdots & A_P(L-1) \end{bmatrix} : L \times P \tag{4.19}$$

$$S = \begin{bmatrix} e^{j\phi_1(0)} & e^{j\phi_1(1)} & \cdots & e^{j\phi_1(M-1)} \\ \cdots & \cdots & \cdots & \cdots \\ e^{j\phi_P(0)} & e^{j\phi_P(1)} & \cdots & e^{j\phi_P(M-1)} \end{bmatrix} : P \times M \tag{4.20}$$

Considering the noise, X will become

$$X = HS + N \tag{4.21}$$

For this X,

- It has full row rank P.

- Each row of S is regarded as a signal from an independent source. All the signals are assumed to be random, independent, identically distributed (i.i.d.).

- The noise is assumed to be additive, white, zero mean, complex Gaussian distributed, with covariance and independent from the sources.

4.3. SINGULAR VALUE DECOMPOSITION (SVD)

The data model after DC removal is X = HS + N where every row of S is an arc, resulting in a complex sinusoidal-like wave which is a linear combination of groups of sine waves with a dominant component, i.e., respiration signal. The statistical independence of common signals are validated in. It has been proved that sine waves of different frequencies are highly independent with each other; therefore, the rows in S can be regarded as independent source signals. The statistics of the above data model are summarized as follows,

The SVD of X is

$$\mathbf{X} = \mathbf{U} \cdot \Sigma \cdot \mathbf{V^H}$$

$$= \begin{bmatrix} \mathbf{U_s} & \mathbf{U_n} \end{bmatrix} \begin{bmatrix} \Sigma_s & \mathbf{0} \\ \mathbf{0} & \Sigma_n \\ \mathbf{0} & \mathbf{0} \end{bmatrix} \begin{bmatrix} \mathbf{V_s^H} \\ \mathbf{V_n^H} \end{bmatrix} \tag{4.22}$$

where U is an L by L unitary matrix containing left singular vectors while V is an M by M unitary matrix containing right singular vectors, S is a diagonal matrix containing all the singular values. The first P columns in U and V are denoted as Us and Vs respectively. The rest columns are denoted as Un and Vn respectively. Indeed, columns of Vs span the same subspace as rows in S and columns of Vn span the null pace as rows in S. Therefore, Us or Vs include the vital sign information of P targets.

4.4. PREVIOUS WORK OVERVIEW

With the previous algorithm [8], we extract the Doppler signals in order to first determine the number of targets and then to estimate their vital signs and location. The first step is to reduce the noise by applying singular value decomposition (SVD) to X. It results is used to determine the number of persons P (target existence probability) in the monitored environment. We specify that in real environments P cannot be determined by simply calculating the rank of X. Knowing the number of targets, the SVD result is further processed by an independent component analysis (ICA) algorithm in order to estimate the sources S . The vital signs information is preserved in the phase information of S. The AC coupling step removes all the DC information of the target, resulting

in a distortion in the phase (angle) extraction. Therefore, we used the linear demodulation algorithm on S to perform phase demodulation in order to extract the vital signs information y(m). At this point, we face an order ambiguity issue: we are still not able to indicate which source (i.e., vital signs signal) corresponds to which subject. H determines the linear combinations of the sources is S , so the magnitudes of the elements in H indicate the energy of the sources in every range bin. Therefore, if we know the propagation channels H of the sources, we can localize the targets and so remove the order ambiguity. From the observation matrix X and the estimated source matrix S, we can then estimate H which is the range information of the targets.
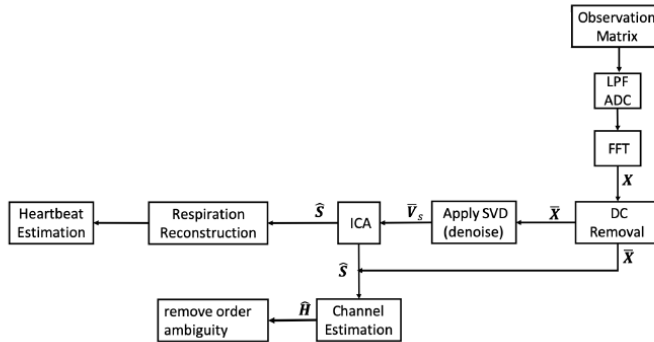
Figure 4.4: Previous algorithm block diagram [8]

4.5. Conclusions

The previous algorithms can estimate the multiple targets' vital sign for the scenario that they are in different range bin. However, when multiple targets are in the same range bin, the previous algorithm does not work. It leads to the extension to the multiple channel radar to use the angular information for the same range bin scenario. The ICA algorithm will not be applied in the proposed one since when applying ICA, it still can not separate the mixed vital sign signals in the same range bin.

5

PROPOSED ALGORITHMS

In this section, the proposed algorithms are discussed in order to detection the target vital signs for the same range bin scenario and find the location (both range and angle) of the targets.

5.1. OVERVIEW OF THE PROPOSED ALGORITHMS

In Figure 5.1, the block diagram of the proposed algorithm is introduced. In the following sections in the chapter, the algorithms will be described in detail which include FFT processing to obtain the range-time-angle radar cube, reconstruction procedure and SVD to obtain the phase values of the vital sign, phase extraction (phase unwrap approach and linear demodulation approach), channel estimation to get the range and angular estimation (DBF and 1D MUSIC).

One example is simulated and tested in each section to show the results. The scenario is shown in Figure 5.2. The range of the direct path is 3.2 meters and at 30 degrees. The ground truth of the simulation for respiration and heartbeat is 0.25Hz and 1.3Hz. Besides the direct path, as discuss in section foure, there will be three different possible multipaths. The mutlipath target are supposed to have the same vital sign frequencies as the real targets.

5.2. FFT PROCESSING

Initially, the 3D data cube are shown as Figure 5.3 and the three dimension of this data cube are in fast time-slow time and sensors. After applying FFT along the fast time, we obtain a new data cube of range, slow time and number of sensors.

Then, the angular information can be extracted through digital beam forming (DBF), which is an advanced approach for steering receiving phased array antennas in order to estimate the angle. Using the data of the same single range-bin over all channels, DBF is conducted through windowing and angular FFT in the sensor-index direction. The radar cube is now in range-time-angle. Figure 5.4 shows the output the FFT processing.
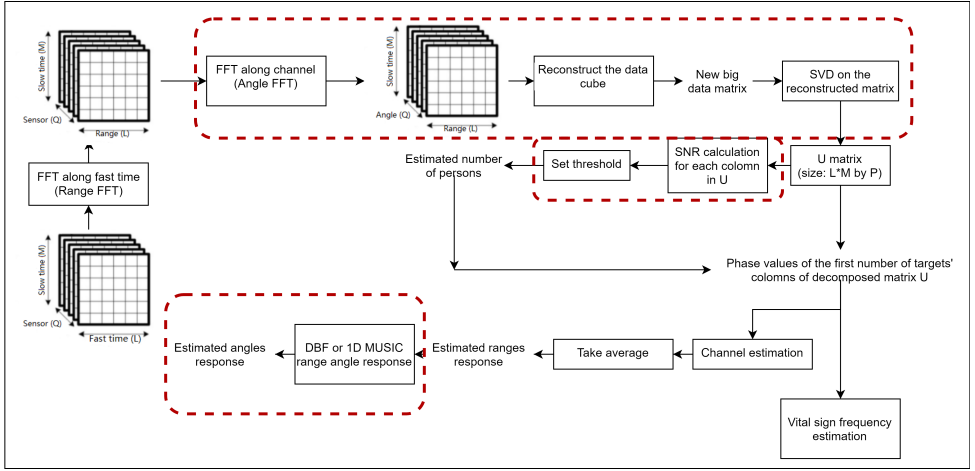
Figure 5.1: Block diagram of proposed algorithm. The additionall angular information of the proposed SIMO frameworks is exploited in the data cube and multiple-channel matrix used as input of the SVD. The SNR metric is defined to estimate the number of targets. Compared to the previous algorithm [8], the red rectangles indicate the novel blocks added in this thesis

5.3. SVD AND TARGET NUMBER ESTIMATION

We first reconstruct the radar data cube (range-time-angle) into a big data matrix $\mathbf{X}_{new}$ which is shown in Figure 5.5. For each angle bin, we have a corresponding range-time matrix. Then, we stack all the corresponding range-time matrix to reconstruct a big data matrix.

The we take SVD on this new constructed data matrix.

$$\mathbf{X}_{new} = \mathbf{U} \cdot \Sigma \cdot \mathbf{V^H}$$
$$= \begin{bmatrix} \mathbf{U_s} & \mathbf{U_n} \end{bmatrix} \begin{bmatrix} \Sigma_s & \mathbf{0} \\ \mathbf{0} & \Sigma_n \\ \mathbf{0} & \mathbf{0} \end{bmatrix} \begin{bmatrix} \mathbf{V_s^H} \\ \mathbf{V_n^H} \end{bmatrix} \tag{5.1}$$

where U is an L by L unitary matrix containing left singular vectors while V is an M by M unitary matrix containing right singular vectors, S is a diagonal matrix containing all the singular values. The first P columns in U and V are denoted as Us and Vs respectively. The rest columns are denoted as Un and Vn respectively. Indeed, columns of Vs span the same subspace as rows in S and columns of Vn span the null pace as rows in S. Therefore, Us or Vs include the vital sign information of P targets. The results of SVD is shown in Figure 5.6. It is proved that after SVD, we can see one clear vital sign signals and the others are noise subspace signals.

Then, the target number estimation algorithm is discussed. In order to estimate target number P, and therefore to determine U_s, we calculate the SNR of the uncorrelated sources in U. A spectrum vital signs signal consists essentially of the respiration fundamental, which is the dominant component of the signal, of one or two decreasing in magnitude respiration harmonics, and of the very small heartbeat fundamental. The
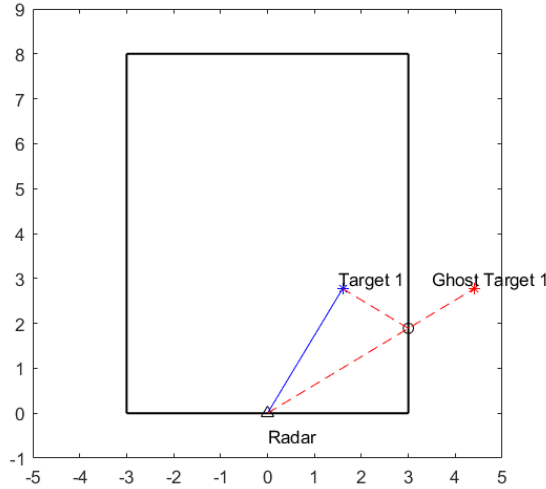
Figure 5.2: Scenario of the example

first P sources of V (i.e., first P columns) produce a high SNR and indicate U_s while the remaining sources have very low SNR and indicate U_n. By using the following SNR definition, we can calculate SNR for each colomn,

$$\text{SNR}_{\text{dB}} = 10\log_{10}\left[\left(\frac{A_{\text{signal}}}{A_{\text{noise}}}\right)^2\right] = 20\log_{10}\left(\frac{A_{\text{signal}}}{A_{\text{noise}}}\right) = \left(A_{\text{signal},\text{dB}} - A_{\text{noise},\text{dB}}\right) \quad (5.2)$$

We perform also other checks on the spectrum's local maxima:

- if the peak, which should indicate the respiration rate, is outside the typical medical ranges, we conclude that this source is noise;

- we determine the ratio of strongest peak and its first harmonic. We consider as noise any source producing a ratio less than 2.

In fact, in the canonical spectrum, the two highest peaks indicate the respiration fundamental and its first harmonic and their ration is always greater than a factor 2. In those two situations, we fix the SNR to 0 dB. The last operation is to scan the obtained SNR profile starting from the first estimation and stopping when the first descending order uncorrelated source produced an SNR below a threshold. The latter source indicates the starting of U_n while the previous ones are the U_s sources corresponding to the P subjects.

5.4. CHANNEL AND RANGE ESTIMATION

In order to estimate the range, we can estimate the H. Since the range information (range bin of the target) can be estimation from the estimated H by finding the largest energy
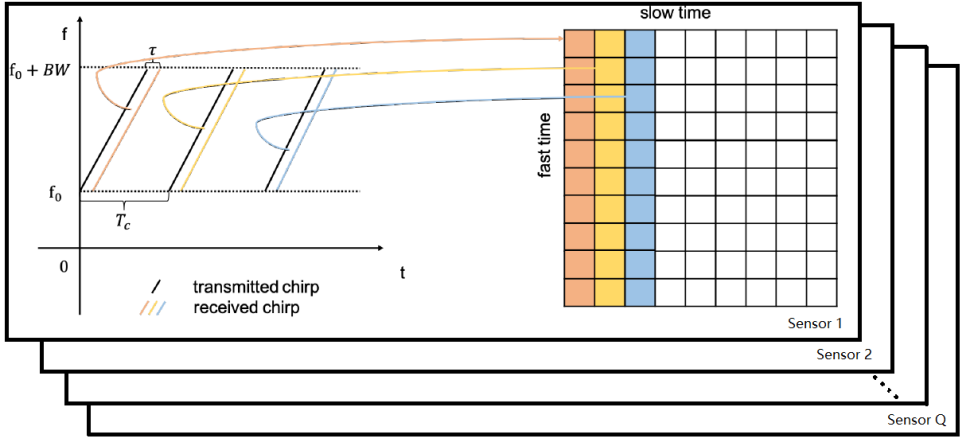
Figure 5.3: Data cube typically extracted from SIMO radar, with range (fast time), slow time, and angle (number of the different sensors or channels)

index.

The channel estimation is used to estimate the range. For each angle bin, we have a range-time observation, X = HS+N.

H determines the linear combinations of the sources in S, so the magnitudes of the elements in H indicate the energy of the sources in every range bin. Therefore, if we know the propagation channels H of the sources, we can localize the targets. From the observation matrix X and the estimated source matrix we can then estimate H.

Now we have already used SVD to obtain the estimated S. We can calculate the estimated H by the following equation by multiplying the pseudo inverse of the previous step estimated S.

$$\widehat{H} = X\widehat{S}^{\dagger} \tag{5.3}$$

5.5. ANGLE ESTIMATION

In this section, two DOA estimation algorithms are discussed. The first one is digital beamforming [18] and the second one is 1D MUSIC [23].

5.5.1. DIGITAL BEAMFORMING (DBF)

Beamforming, also known as spatial filtering, is a kind of technology that focus the radar beam of antenna array to some desired direction over azimuth or elevations. In an antenna array, beamforming is realized through summing up the weighted signals of each elements, the weighting basically includes information of amplitude and phase. As a result, signals at a specific direction will be constructively interfered and thus a narrow beam will be directed to the angle of interest.

In a ULA SIMO radar system, the phase difference between two adjacent antennas can be shown as:
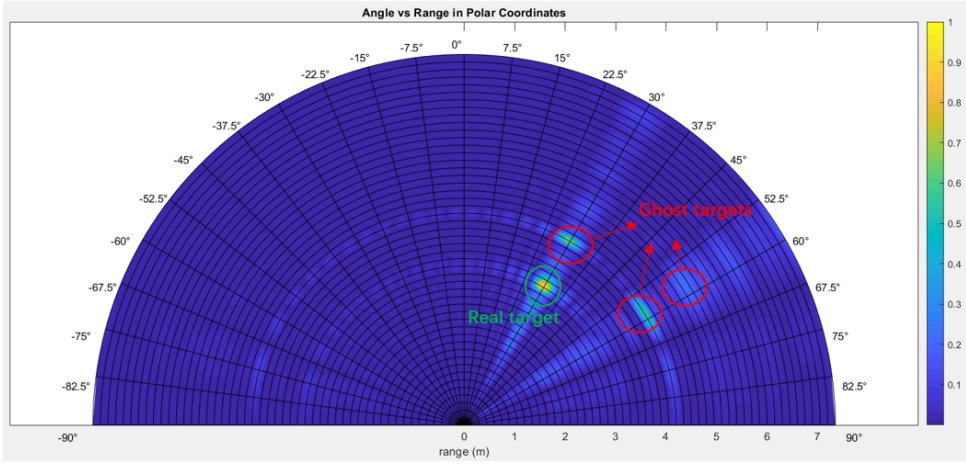
Figure 5.4: Range angle results of the FFT processing of one time slice

$$\Delta\phi = \frac{2\pi d \sin(\theta)}{\lambda} \tag{5.4}$$

Assume the baseband signal of Rx1 is $S_B(t)$. The other signals at different Q sensors can be formulated as

$$X_i(t) = S_B(t)e^{j(i-1)\Delta\phi} \tag{5.5}$$

And the results after using DBF techniques is:

$$S_i(t) = \sum_{i=1}^{Q} W_i X_i(t) \tag{5.6}$$

In order to make the same-direction addition of $S_i(t)$, the phase difference of each RF chain needs to be removed. Therefore, the coefficient W_i can be expressed as:

$$W_i = e^{-j(i-1)\Delta\phi} \tag{5.7}$$

The spatial results of DBF are shown in Figure 5.9.

5.5.2. 1D MUSIC
According to the number of detected targets, the noise subspace can be extracted from the eigen decomposition as

$$\mathbf{U}_{\bar{k}} = \left[\mathbf{W}_{\bar{k}}\mathbf{V}_{\bar{k}}\right] \tag{5.8}$$

where $\mathbf{V}_{\bar{k}}$ and $\mathbf{V}_{\bar{k}}$ represent the signal subspace and noise subspace, respectively.

Divide the angle domain into Q grids as $[\theta_0, \theta_1, ..., \theta_Q]$ and formulate the steering vector a(θ)
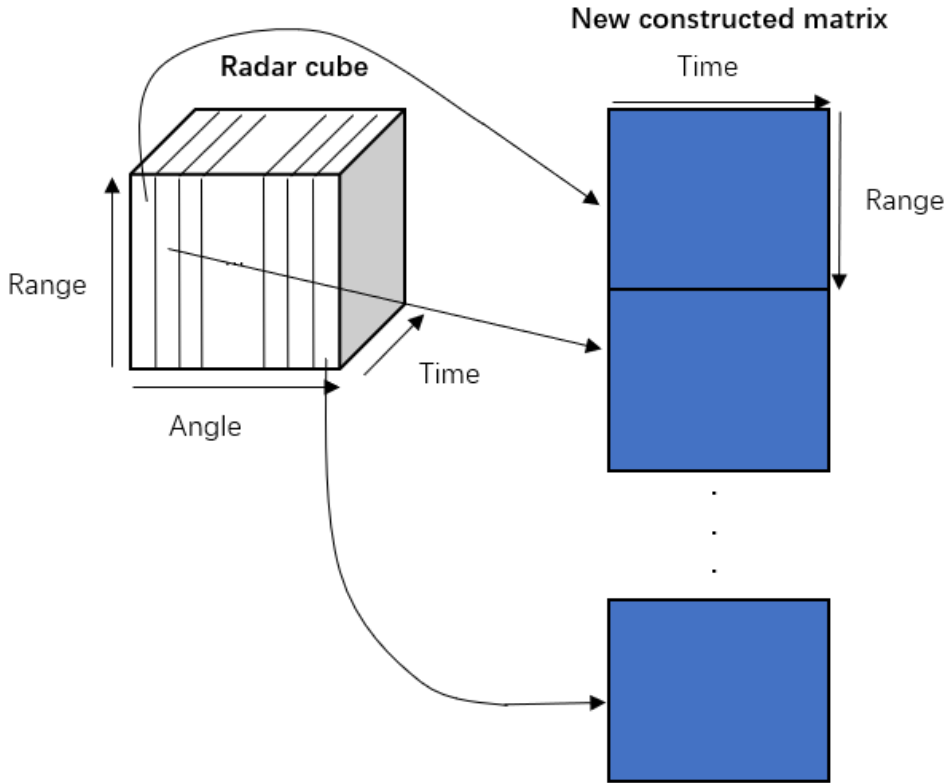
Figure 5.5: The idea of construction the data cube into a new data matrix

where d is the inter space between neighbouring elements and λ is the wavelength of the center frequency. Applying MUSIC algorithm, the pseudo-spectrum of angle can be obtained.

$$p_{\tilde{k}} = \left[\frac{1}{\left\| \mathbf{a}\left(\theta_0\right)\mathbf{V}_{\tilde{k}}\right\|^2}, \cdots, \frac{1}{\left\| \mathbf{a}\left(\theta_Q\right)\mathbf{V}_{\tilde{k}}\right\|^2} \right]^T \tag{5.9}$$

The spatial results of 1D MUSIC are shown in Figure 5.9.

5.6. PHASE EXTRACTION

In this section, two phase extraction methods are discussed in the context of vital signs monitoring, i.e. in order to use the phase information to estimate the respiration and heartbeat rates.
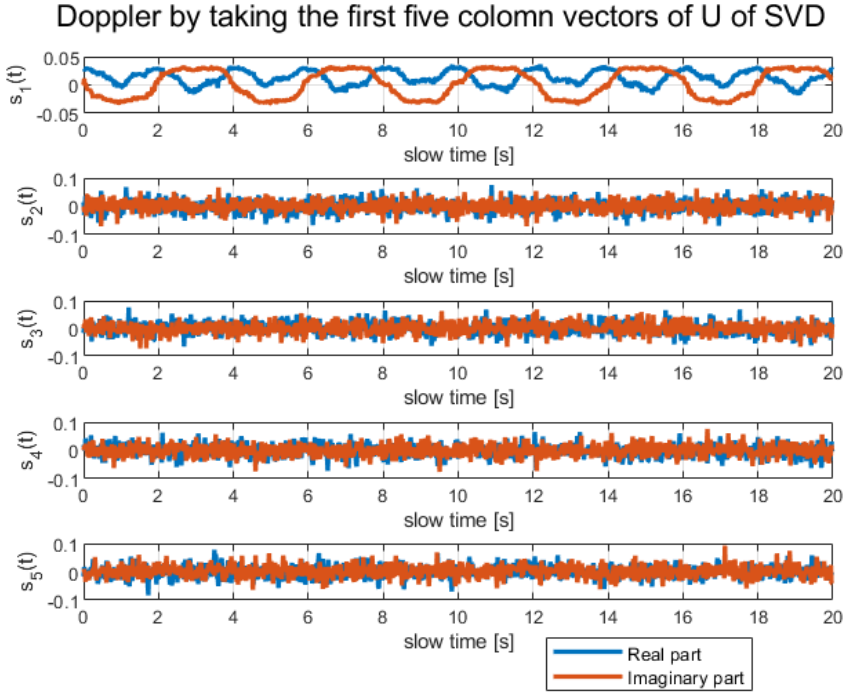
Figure 5.6: SVD results which shows dopplers by taking the first five colomn vectors of U after SVD

5.6.1. PHASE UNWRAPPING

Extract the phase of signal $\mathbf{s}[n]$, we get the phase history ϕ_i. After obtaining the phase information ϕ_i of the desired signal, the 2π discontinuity of the extracted phase appears when an extreme value, $\pi/-\pi$, is reached; the phase then jumps to the other end of the interval, $-\pi/\pi$, which suffers from the deficiency known as phase wrapping. To tackle this problem, the unwrapping process is necessary to avoid the jump of the extracted phase, the process steps are:

1. Calculate the difference between the current sample in wrapped phase signal $\phi_w(n)$ and its previous adjacent phase sample $\phi_w(n-1)$:

$$\Delta\phi = \phi_w(n) - \phi_w(n-1), \qquad n = 2,\ldots,N \tag{5.10}$$

2. If $\Delta\phi > +\pi$, subtract 2π from current phase sample and also from all the samples to the right of it.

3. If $\Delta\phi < -\pi$, add 2π to the current sample and also to all the samples to the right of it.

The process can be mathematically expressed as:

$$\phi_u(t) = \mathscr{U}[\phi_w(t)] = \phi_w(t) + 2\pi k, \qquad k \in \{-1,1\} \tag{5.11}$$
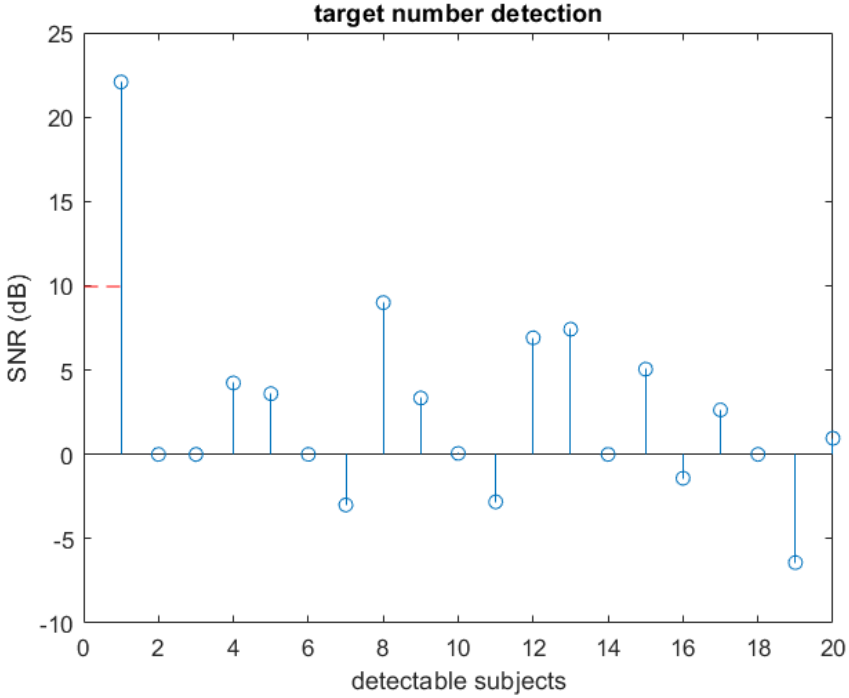
Figure 5.7: SNR results to show how the target number is estimated

where $\mathcal{U}[\cdot]$ indicates the phase unwrapping operation, then phase history $\phi_{his}(t)$ can be obtained as:

$$\phi_{his}(t) = \mathcal{U}[\phi_i(t)]. \tag{5.12}$$

The results of phase unwrapping can be found in Figure 5.11

5.6.2. LINEAR DEMODULATION

The vital signs information is preserved in the phase information of S. The AC coupling step used to obtain removes all the DC information of the target, resulting in a distortion in the phase (angle) extraction. Therefore, we used the linear demodulation algorithm on S to perform phase demodulation in order to extract the vital signs information.

Based on the small angle approximation, a vital sign source can be approximated as:

$$s(t) = e^{j\emptyset(t)} \approx 1 + j\emptyset(t) - \frac{\emptyset^2(t)}{2} \tag{5.13}$$

where is the phase (Doppler) shift caused by the vital signs. After DC removal, it becomes:

$$\bar{s}(t) \approx j\emptyset(t) - \frac{\emptyset^2(t)}{2} \tag{5.14}$$
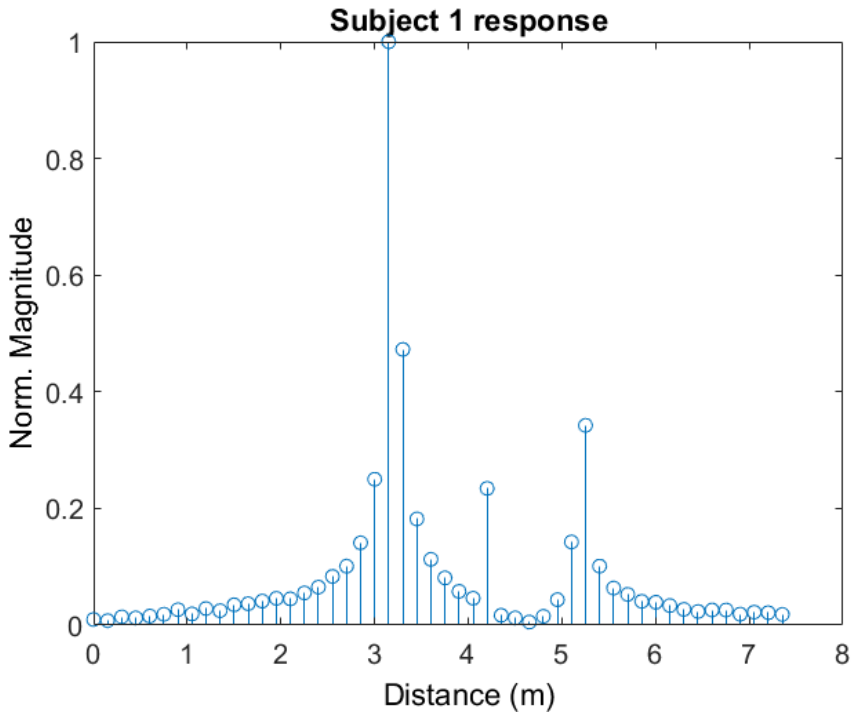
Figure 5.8: Channel estimation results which show the magnitudes of the energy of the sources in every range bin.

where the two terms are orthogonal and the imaginary part is more powerful than the real part. The vital signs information y (t) can be extracted from the estimated source s (t) after linear demodulation and it can be expressed as:

$$\hat{y}(t) = \hat{s}(t) \frac{\lambda_0}{4\pi} \tag{5.15}$$

where λ_0 is the wavelength corresponding with the start frequency of the chirp. If the demodulation is performed correctly, the above equation is equivalent to the motion of the chest surface R(t) caused by the vital signs.

The results of linear demodulation can be found in Figure 5.11

5.7. VITAL SIGN FREQUENCY ESTIMATION

Two signal decomposition methods are discussed in this section which are wavelet decomposition and EMD. After separating the respiration and heartbeat, the FFT and peak detection are applying to find the estimation respiration rate and heartbeat rate.

(a) DBF   (b) 1D MUSIC
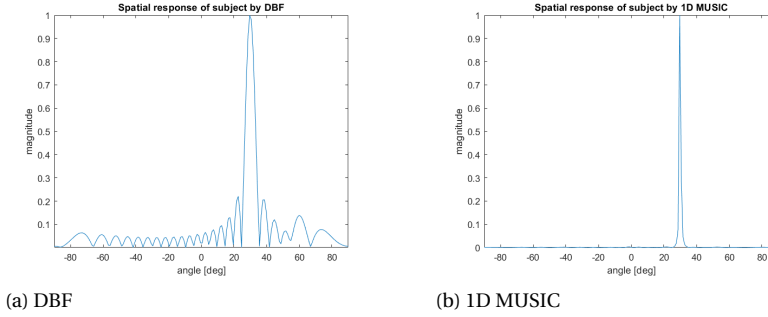
Figure 5.9: Angle estimation spatial response by using DBF and 1D MUSIC
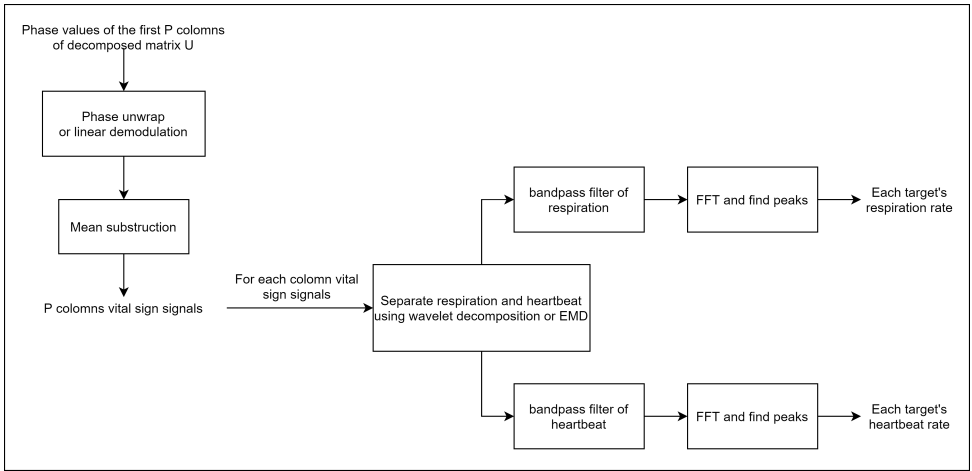
Figure 5.10: Vital sign estimation block diagram

5.7.1. WAVELET DECOMPOSITION

Wavelet transform offers variable time-frequency resolution. The finite oscillatory nature of wavelets makes wavelet transform extremely useful for nonlinear and nonstationary signals in real life situations. Suppose sampling frequency of x(t) is f , L-level discrete wavelet decomposition coefficients are

$$\left[c_1^L \cdots c_{\frac{N}{2^L}}^L : d_1^L \cdots d_{\frac{N}{2^L}}^L \vdots \cdots d_1^2 \cdots d_{\frac{N}{4}}^2 \vdots d_1^1 \cdots d_{\frac{N}{2}}^1 \right] \tag{5.16}$$

where c_i^r and d_i^r are approximation coefficients and detail coefficients at the level r scaling, respectively, and N is the length of x(t). The frequency range of the rth level detail coefficients is from f/2^r to f/2^r − 1 .

The results of EMD are shown in Figure 5.12.

(a) Phase unwrap   (b) Linear demodulation
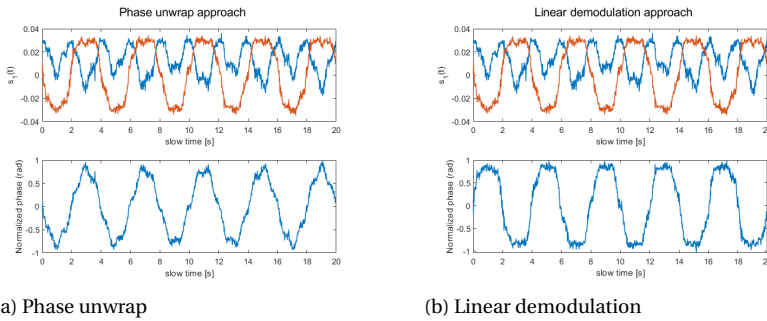
Figure 5.11: Phase extraction by using phase unwrapping or using linear demodulation

5.7.2. EMD

EMD deconstructs non-stationary and non-linear signals into a set of mono-component signals called intrinsic mode functions (IMF). An IMF is a function that represents the oscillation mode embedded in the data signal. An IMF satisfies 2 conditions: the number of extrema and zero crossings must be either equal or differ by one, and the mean value of the envelope defined by the local maxima and the envelope defined by the local minima is zero.

Similar to wavelet analysis, EMD decomposes the signal into IMFs of different resolution scales. However, in EMD, the basis functions are directly extracted from the data, while in wavelet analysis, a pre-designed mother wavelet is selected before the analysis and determines the basis functions for the different scales. Therefore, IMF can better represent the local characteristics of a signal, and adapt to the signal's oscillation patterns over time. Due to this advantage, EMD is suitable for analyzing nonlinear and non-stationary signals. A real valued signal y(t) can be represented as a set of IMFs plus a residual:

$$y(n) = \sum_{k=1}^{N} s_k(n) + r_k(n) \quad k = 1, 2, \ldots, N \tag{5.17}$$

where $s_k(n)$ are the resulting IMFs and $r_k(n)$ the residual term.

The results of EMD are shown in Figure 5.12.

5.8. CONCLUSIONS

Figure 5.13 shows the final estimated frequencies of one targets compared to the ground truth. It can be seen that final estimation with proposed algorithm can still work for the multipath scenario. While we want to further discover how the angular information helps the vital sign estimation and target localization compared to the SISO FMCW radar which previous work used. Therefore, in the next section of case tests, we simulated two targets in the same range bin in order to figure out it.
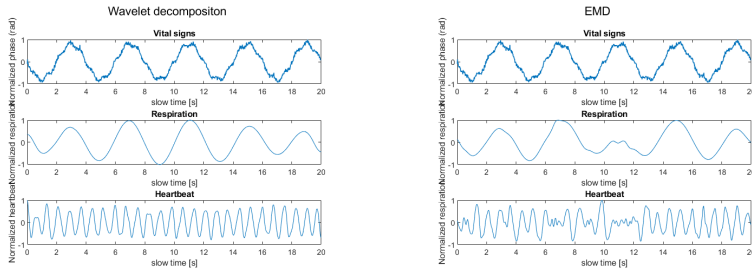
(a) Wavelet   (b) EMD

Figure 5.12: Wavelet decomposition and EMD results

5
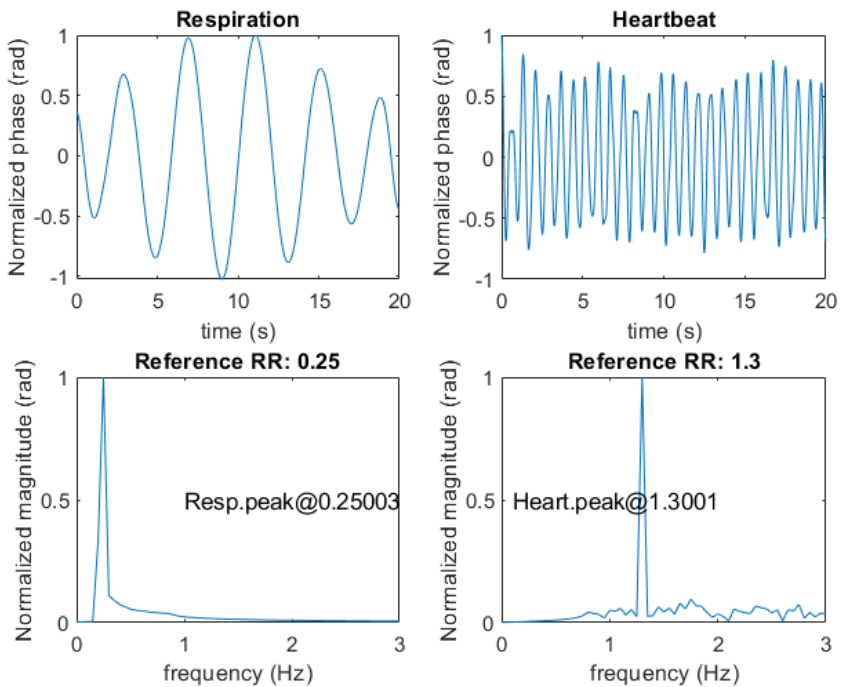
Figure 5.13: Vital sign estimation results compared to the ground truth

6

CASE SIMULATION TESTS

In this section, two case tests are simulated based on the same configuration of the radar parameters. We present two cases whose characteristics are summarised below: 1) two subjects with the same range and different respiration and heartbeat frequencies without considering the multipath effect; 2) two subjects with the same range and different respiration and heartbeat frequencies with considering the multipath effect

6.1. CONFIGURATION OF THE SIMULATIONS

FMCW Signal generation is realized based on MATLAB which built the signal model fixed with realistic data collected by the IMEC radar [17]. The parameters of simulated FMCW chirp signal is shown in Table 6.1.

The simulated model uses 24 spatial channels for DOA estimation (formed by 1 transmitters and 24 receivers MIMO array), 1111 slow-time snapshots for Doppler processing and 512 fast-time snapshots for range processing. Each transmitter emits FMCW signals (IF signal) modulated to center frequency (RF signal) sequentially to generate Time Division orthogonal waveforms. The received signals are generated by timedelayed transmitted signals. The delay is calculated. To generate reflected echo from targets, radar range equation is calculated to get the received power as follows

$$P_r = \frac{P_t G_t G_r \lambda^2 \sigma}{(4\pi)^3 R^4 L} \tag{6.1}$$

where P_r ,P_t are the received and transmitted power, G_t ,G_r are transmitter and receiver gain, σ is target's nonfluctuating radar cross section in square meters, R is the distance from radar to the target, and L is the general loss factor.

Then the complex conjugate of down-converted received signal (IF signal) is multiplied with transmitted signal to generate deramped signal for processing. After deramping, the bandwidth of the signal is reduced considerably which allows lower sampling frequency.

Radar parameter	Values
Centre frequency	7.3 GHz
Bandwidth	1GHz
Chirp duration	40.96 ns
PRI (pulse repetition interval)	40.96 ns
Observation frame period	20 s
Number of channels	24 channels

Table 6.1: Parameter of the radar

6.2. CASE TEST A: TWO TARGETS IN THE SAME RANGE BIN WITH-OUT MULTIPATH EFFECT

In the case test, the scenario is show in the Figure 6.1. Since in this case, the multipath effect is not supposed. It should output relatively good result. The ground truth data are two targets both at 3.6m. RR for target 1 is 0.32Hz and HR for target 1 is 1.5Hz at 30 degrees. RR for target 2 is 0.23Hz and HR for target 2 is 1.1Hz at -45 degrees. The other estimation reults are shown in the other figures. The input ground truth data are applied to the SISO radar at the same time for comparison with SIMO one. Figure 6.2 shows the range angle plots of a time slice according to the scenario. Figure 6.3 shows that vital sign, location and angle estimation of two targets with comparing the ground truth (in red line). From Figure 6.4 and Figure 6.5, we compared the estimated respiration frequency and heartbeat frequency of both targets with the ground truths.

To compare with the SIMO results, the same range and vital sign ground truth are used to generate the SISO data. It can been seen from Figure 6.6 the range time plot are shown. Figure 6.7 shows that vital sign, location and angle estimation of two targets with comparing the ground truth (in red line). From Figure 6.8 and Figure 6.9, we compared the estimated respiration frequency and heartbeat frequency of both targets with the ground truths.

6.3. CASE TEST B: TWO TARGETS IN THE SAME RANGE BIN WITH MULTIPATH EFFECT

In the case test, the scenario is show in Figure 6.10. Since in this case, we suppose the multipath effect. For one real target, all the three possible multipath possibilities are supposed in this case test. The ground truth data are two targets both at 3.6m. RR for target 1 is 0.24Hz and HR for target 1 is 1.2Hz at 30 degrees. RR for target 2 is 0.31Hz and HR for target 2 is 1.8Hz at -45 degrees. The other estimation reults are shown in the other figures. The input ground truth data are applied to the SISO radar at the same time for comparison with SIMO one. Figure 6.11 shows the range angle plots of a time slice according to the scenario. Figure 6.12 shows that vital sign, location and angle estimation of two targets with comparing the ground truth (in red line). From Figure 6.13 and Figure 6.14, we compared the estimated respiration frequency and heartbeat frequency of both targets with the ground truths.
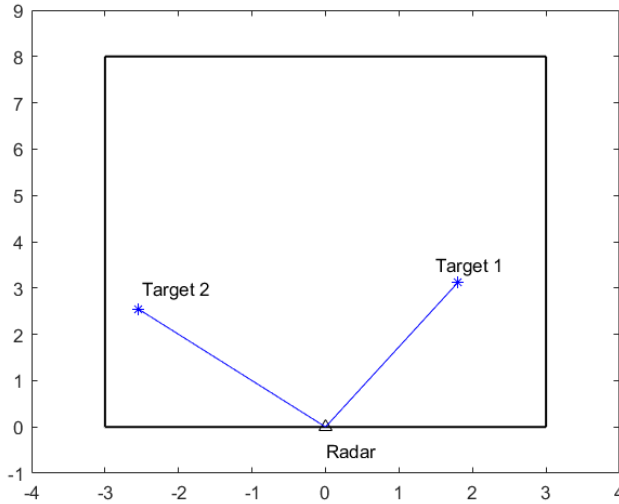
Figure 6.1: sketech of case A scenario where two subjects with same distance and different angle are shown

To compare with the SIMO results, the same range and vital sign ground truth are used to generate the SISO data. It can been seen from Figure 6.15 the range time plot are shown. Figure 6.16 shows that vital sign, location and angle estimation of two targets with comparing the ground truth (in red line). From Figure 6.17 and Figure 6.18, we compared the estimated respiration frequency and heartbeat frequency of both targets with the ground truths.

6.4. Conclusions

In conclusion, with the proposed algorithms, the multipath effect can be removed. And SIMO radar can work for the same range bin scenario with the angular information, while SISO radar can not. In the same range bin of SISO radar, two vital signs of different targets are mixed together which are difficult to separate two targets' vital sign.

In order to generalise this performances as an alternative to the experiments validation that can not be performed, the Monte Carlo simulations are conducted.
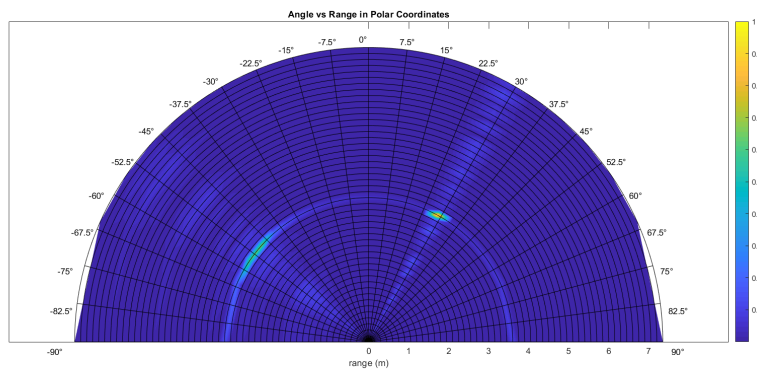
Figure 6.2: Range time plot of a time slice for scenario A where there are two subjects at the same distance and different angle

6
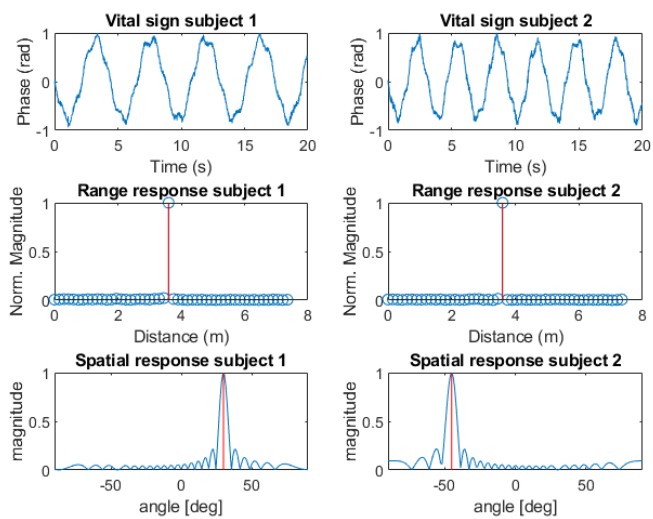
Figure 6.3: Vital sign, location, and angle estimation of subject 1 and subject 2 (red lines are ground truth) (SIMO)
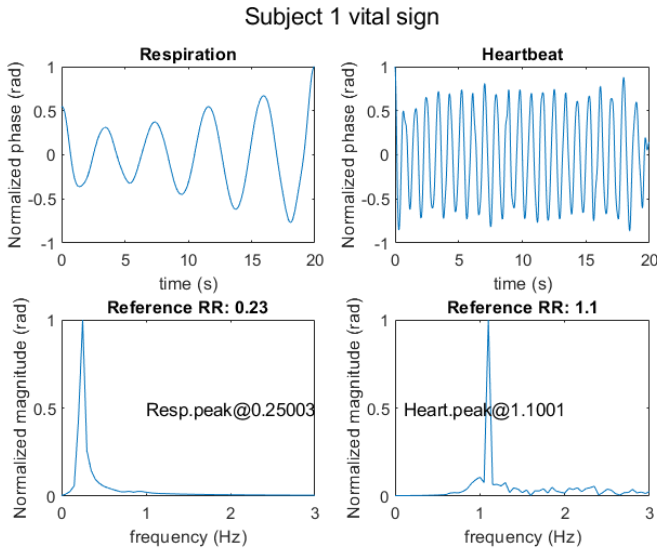
Figure 6.4: RR and HR estimation of subject 1 (SIMO) and the correct vital sign is well estimated
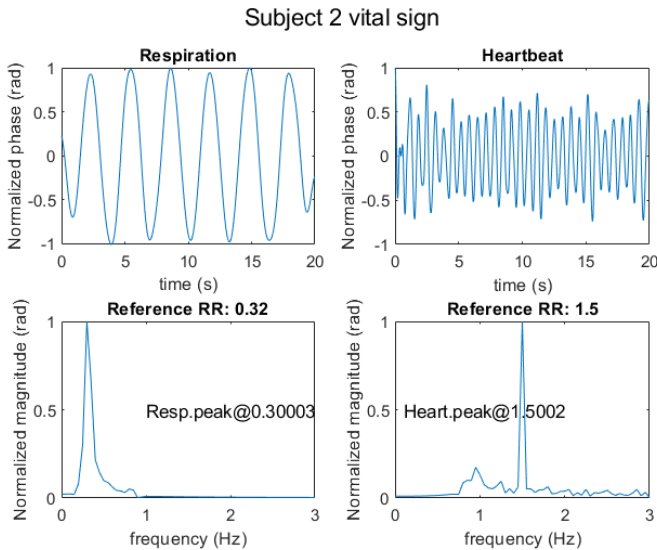
Figure 6.5: RR and HR estimation of subject 2 (SIMO) and the correct vital sign is well estimated

6
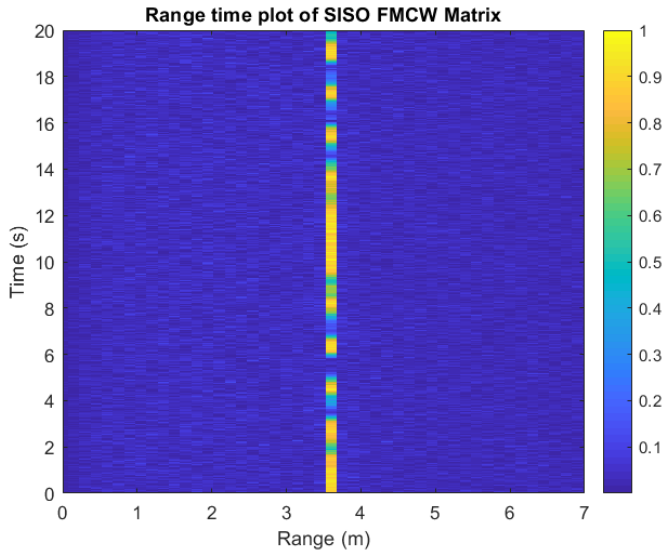
Figure 6.6: SISO range time plot for scenario A where there are two subjects at the same distance and different angle

6
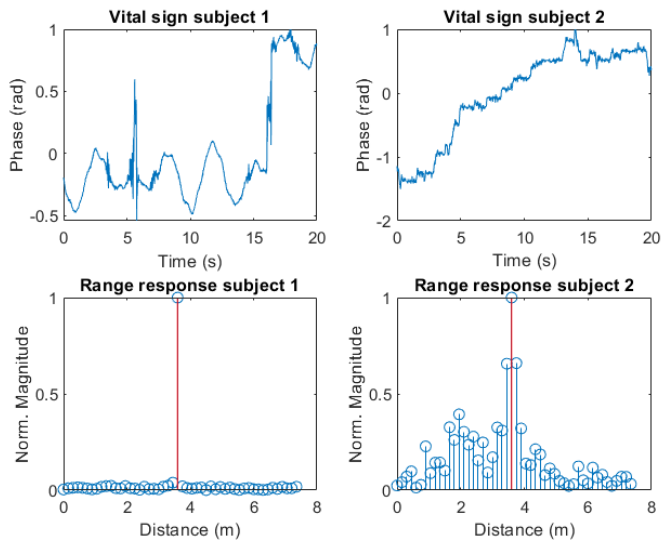
Figure 6.7: Vital sign, location estimation of subject 1 and subject 2 (red lines are ground truth) (SISO)
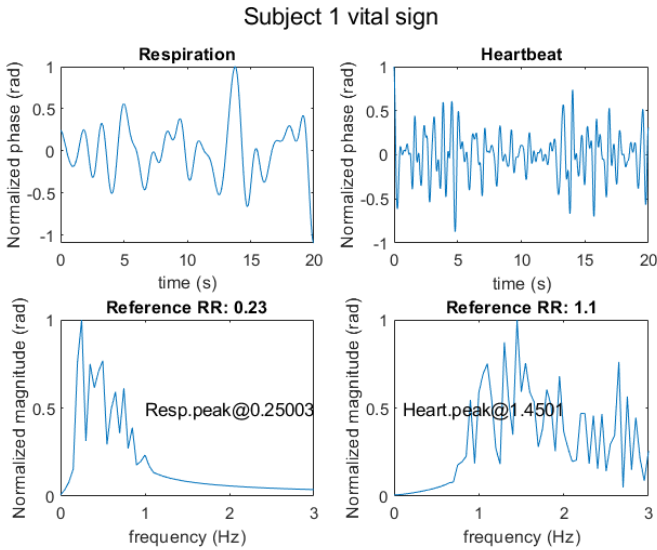
Figure 6.8: RR and HR estimation of subject 1 (SISO), the estimation does not work well for subject 1, especially estimating HR
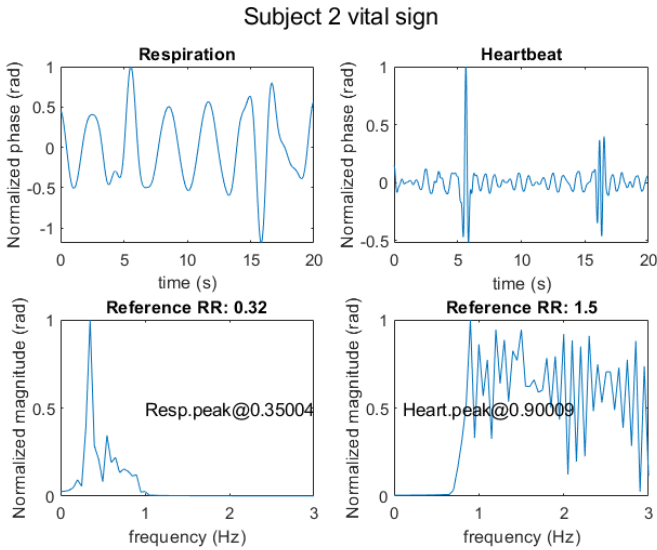
Figure 6.9: RR and HR estimation of subject 2 (SISO), the estimation does not work well for subject 2, especially estimating HR
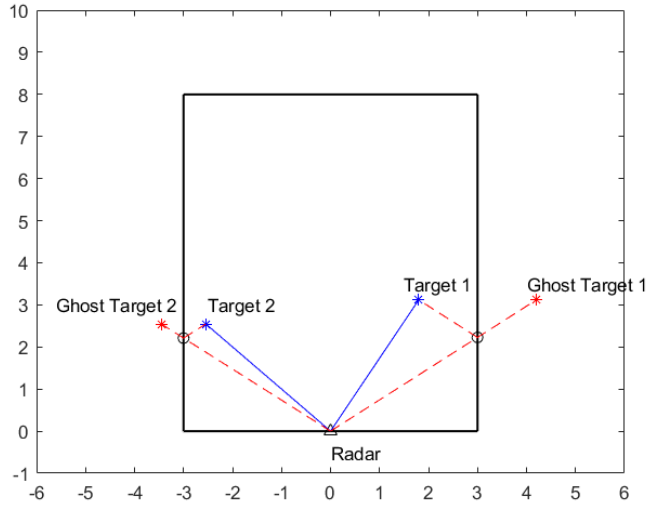
Figure 6.10: Scenario of this case B scenario with considering the multipath effect where two subjects with same distance and different angle are shown
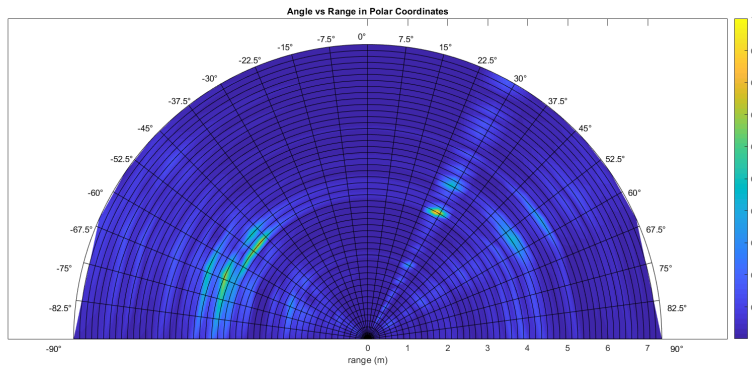
Figure 6.11: Range time plot of a time slice for case B scenario with considering the multipath effect where two subjects with same distance and different angle, the figure gets more complicated and there are ghosts due to multipath
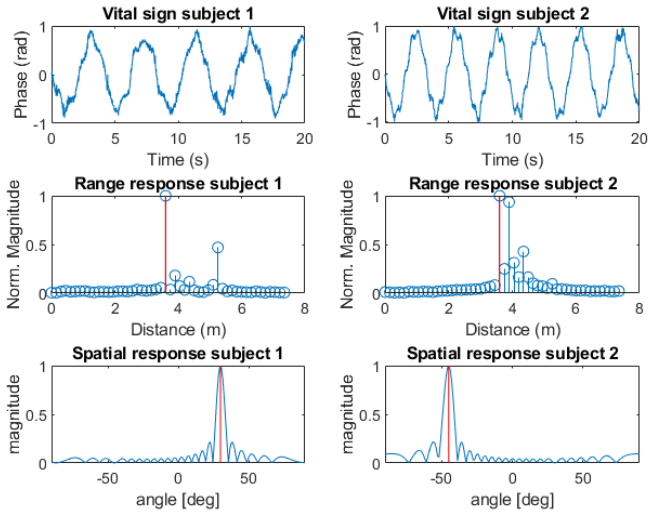
Figure 6.12: Vital sign, location, and angle estimation of subject 1 and subject 2 (red lines are ground truth) (SIMO), works well for the estimation
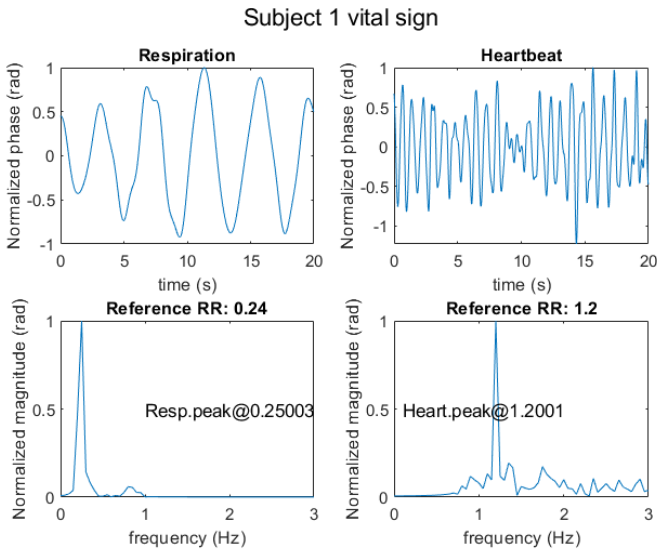
Figure 6.13: RR and HR estimation of subject 1 (SIMO), works well for the estimation
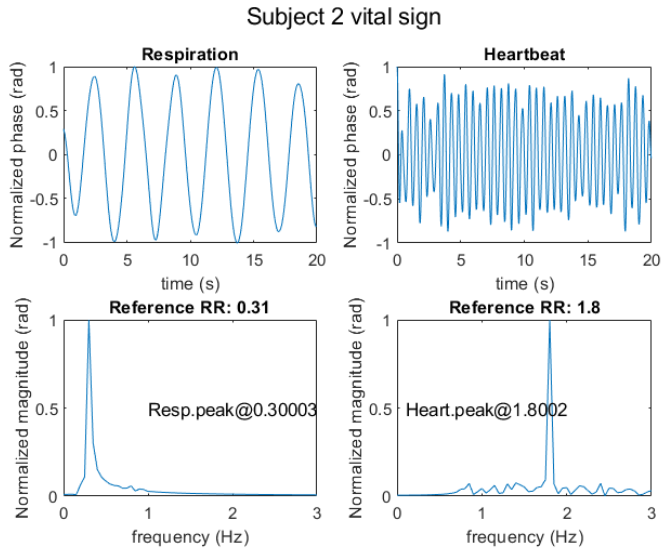
Figure 6.14: RR and HR estimation of subject 2 (SIMO), works well for the estimation

6
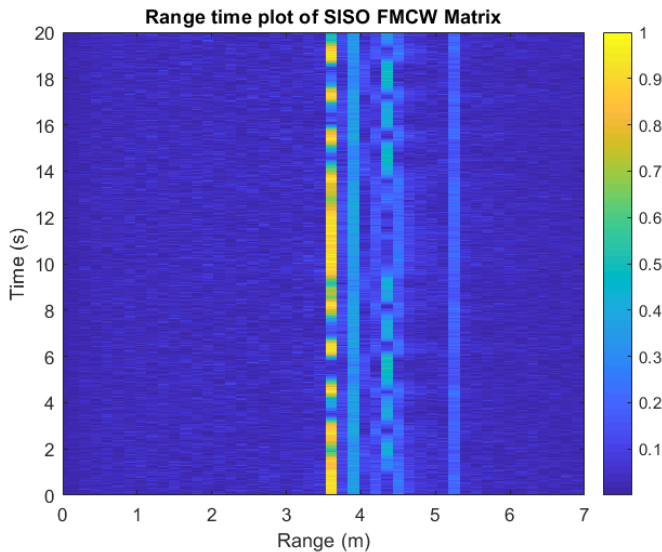
Figure 6.15: SISO range time plot for case B scenario with considering the multipath effect where two subjects with same distance and different angle
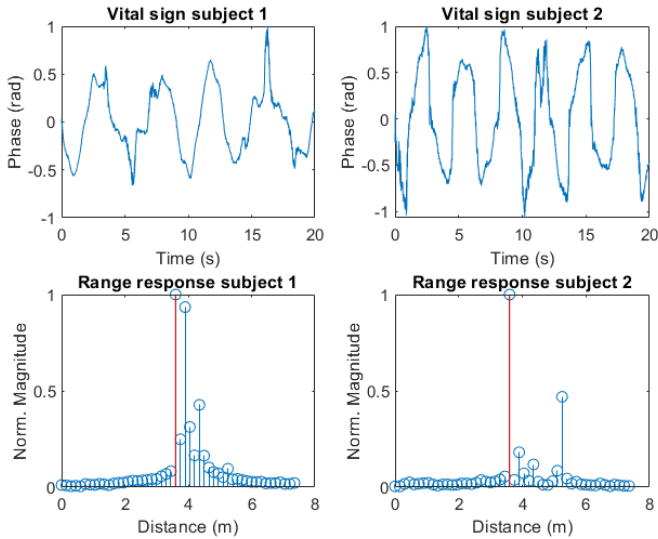
Figure 6.16: Vital sign, location estimation of subject 1 and subject 2 (red lines are ground truth)

6
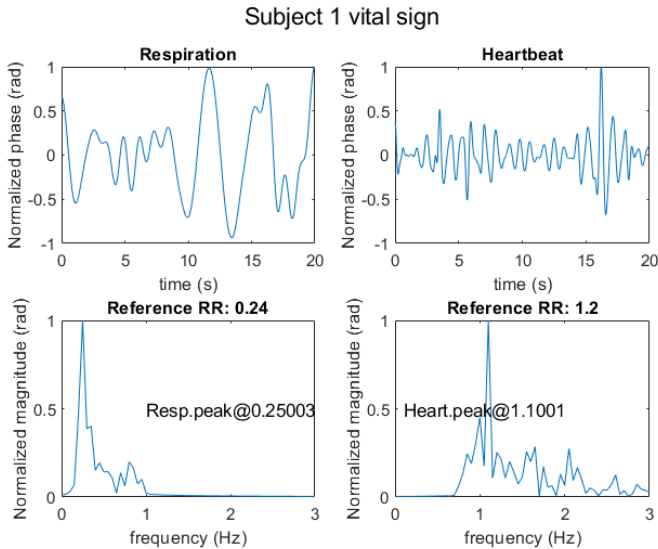
Figure 6.17: RR and HR estimation of subject 1 (SISO), HR is a bit wrong estimated
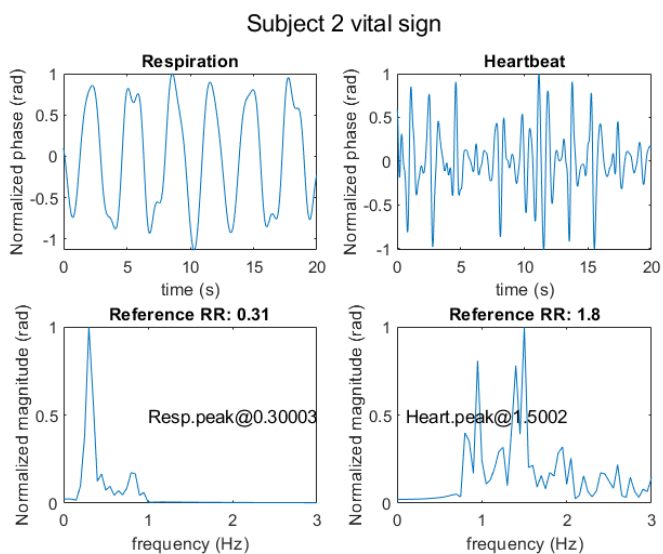
Figure 6.18: RR and HR estimation of subject 2 (SISO), HR is wrongly estimated

7

MONTE CARLO SIMULATIONS

In this chapter, the Monte Carlo simulation is conducted for generalising this performances as an alternative to the experiments validation that can not be performed

7.1. RESULTS OF MONTE CARLO SIMULATION FOR TARGETS IN THE SAME RANGE BINS

50 sets of random data with initialising two targets in the same range bin, the summary of the generation for each data are described as follows:

- Two subjects are 1 meter and 4 meters and between 30 degrees and -45 degrees

- Their vital signs are also randomly initialised between the value according to the review table Table 3.1.

- one ghost target is simulated with the same vital sign information of target 1 and in the range between 5 meter to 6 meter at 60 degree

Overall results which are the difference between the ground truth value and the estimated value of location, respiration rate and heartbeat rate are shown in the following table. Table 7.1 summarises the results of the 50 MC simulations in terms of mean error and standard deviation of the error between the estimated value of key parameters and their actual value. The histograms plot in the subsequent figures show the distribution of the amount of this error.

It can been seen that the mean error values of the heartbeat rate estimation are very large. It is because that in SISO it could not detect the two subjects at all for the heartbeat rate. Since it was not visible without the angular differentiation

7.1.1. LOCATION DIFFERENCE BETWEEN SISO AND SIMO

From Figure 7.1 and Figure 7.2, we can see SIMO have a better performance than SISO, especially for the estimation of subject 2 location.

	SISO mean error	SISO STD of error	SIMO mean error	SIMO STD of error
Location S1(m)	0.0515	0.0304	0.0793	0.0451
Location S2(m)	0.5146	0.6157	0.1358	0.4299
Respiration S1 (bpm)	1.1606	1.5764	0.8099	0.5648
Respiration S2 (bpm)	1.8632	2.2452	0.7932	0.4660
Heartbeat S1 (bpm)	44.3687	27.3391	0.9870	0.9876
Heartbeat S2 (bpm)	16.1341	18.8573	0.7210	0.4235

Table 7.1: Monte Carlo simulation reults overview

For the first subject, both SISO and SIMO have a good estimation and SISO could even works better than SIMO since for the SIMO channel (range) estimation, we take an average value for each sensor's estimation. While, for the second subject, SIMO radar shows a better results than SISO for much more Monte Carlo experiments in less in 0.15 meters.

7

(a) SISO location difference histogram

(b) SIMO location difference histogram
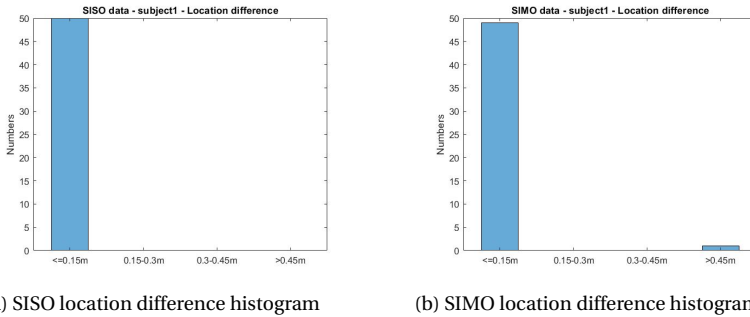
Figure 7.1: Location difference compared to the input ground truth between SISO and SIMO for subject 1

7.1.2. Respiration rate difference between SISO and SIMO

From Figure 7.3 and figure Figure 7.4, we can see SIMO have a overall superior performance than SISO for estimating the respiration rate.

For the first subject, SIMO is slightly better than SISO radar. While for the second subjects, SIMO works much better with all the respiration difference compared to the ground truth between 0 to 2 bpm.

(a) SISO location difference histogram

(b) SIMO location difference histogram
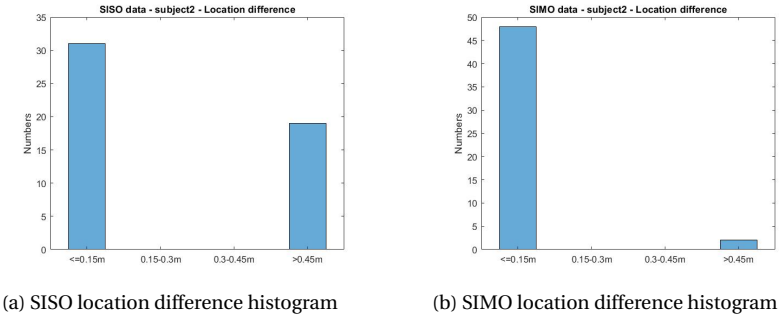
Figure 7.2: Location difference compared to the input ground truth between SISO and SIMO for subject 2

(a) SISO RR difference histogram

(b) SIMO RR difference histogram
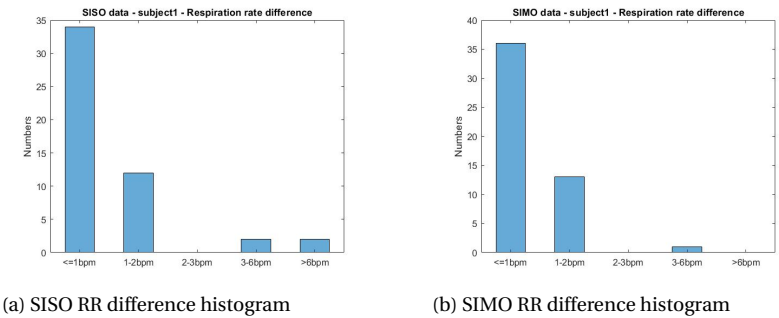
Figure 7.3: RR difference compared to the input ground truth between SISO and SIMO for subject 1

7.1.3. HEARTBEAT RATE DIFFERENCE BETWEEN SISO AND SIMO

From Figure 7.5 and figure Figure 7.6, we can see SIMO have a overall higher quality performance than SISO for estimating the heartbeat rate.

For the first subject, SIMO is really better than SISO radar. And SISO radar has very limited Monte Carlo simulations to have a relatively correct result. While for the second subjects, SIMO works much better with all the respiration difference compared to the ground truth between 0 to 2 bpm while SISO not.

7.2. CONCLUSIONS

In conclusion, SIMO have a better performance than SISO in vital sign estimation and target localization for the same range bin scenario. It is also proved than the angular information can help for this same range bin scenario.
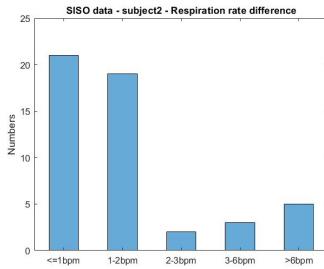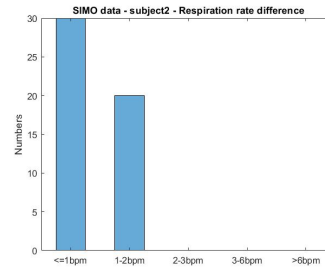
(a) SISO RR difference histogram   (b) SIMO RR difference histogram

Figure 7.4: RR difference compared to the input ground truth between SISO and SIMO for subject 2
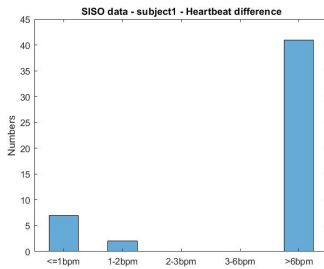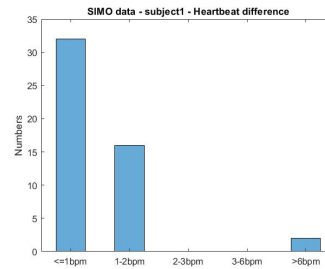
(a) SISO HR difference histogram   (b) SIMO HR difference histogram

Figure 7.5: HR difference compared to the input ground truth between SISO and SIMO for subject 1
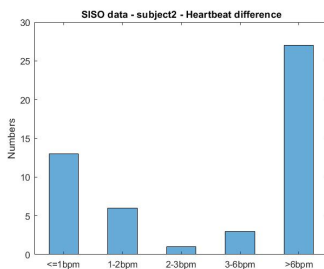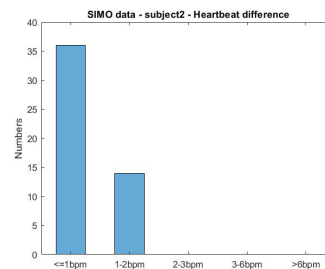
(a) SISO HR difference histogram   (b) SIMO HR difference histogram

Figure 7.6: HR difference compared to the input ground truth between SISO and SIMO for subject 2

<div align="right"># 8</div>

CONCLUSION AND FUTURE WORK

8.1. CONCLUSION

The aim of this MSc thesis was to explore the data processing algorithms for radar-based non-contatct long term health monitoring (i.e., HR and RR) and the possibility of realizing indoor positioning at the same time. This is in-line with the growing demand for non-contatct health monitoring in hospitals, schools, homes and cars. The main research activities aimed to extend the work of a previous master thesis from SISO (single input single output) radar to a SIMO (single input multiple output) radar framework. The core idea is that the usage of multiple receiver channels that SIMO radar provides can enable an additional degree of freedom (the estimation of the angular position) to distinguish real targets from ghost targets due to multipath, hence improving their rejection and cancellation. Simulation results are then generated to compare SISO and SIMO frameworks for recognition of the number of subjects in a given environment, for their localisation, and for the estimation of their vital signs.

The key contributions of this thesis work are summarised in the following bullet points.

- Detailed analysis of the multipath effects for the problem of vital signs indoor estimation, with key assumptions in the developed model.

- Construction and full characterisation of the SIMO radar data cube for further processing in the range-Doppler-angle domain.

- Formulation of angular localisation algorithm as part of vital signs estimation process for multiple subjects in SIMO radar framework.

- New definition of an SNR metric for the estimation of the number of subjects

- Validation and comparison of performances of SISO and SIMO vital sign estimation

The effectiveness of the proposed approach has been demonstrated via simulations, in particular a Monte Carlo simulations with multiple subjects located at the same range bin but at different azimuth angle and with different vital signs. The proposed SIMO framework achieved a reduction of error in the estimated location parameters of about 0.3m with respect to the conventional SISO case. The proposed SIMO framework achieved a reduction of error in the estimated respiration rate parameters of about 1.4bpm with respect to the conventional SISO case. The proposed SIMO framework achieved a good estimation of heartbeat parameters, while the conventional SISO case can not output a reliable heatbeat frequency estimation.

8.2. RECOMMENDATIONS OF FUTURE WORK

Unfortunately, due to access limitation caused by the COVID-19 pandemic to the offices of IMEC, Eindhoven, where this thesis work was mostly performed, the initially planned experimental validation with SIMO radar was not possible to perform. Therefore, the first future work is to collect real data with a SIMO FMCW radar in the indoor environment.

For signal decomposition method, some other real time techniques such as online-EMD or online VMD could be applied in order to get a better computational performance and also better for the algorithms in the real time embedded system.

Now the indoor environment multipath effect are supposed to be 2D, while in the real environment, it will be a 3D environment. Then, the geometry of the multipath effect will be more complicated.

8

BIBLIOGRAPHY

[1] Marco Mercuri et al. "Vital-sign monitoring and spatial tracking of multiple people using a contactless radar-based sensor". In: *Nature Electronics* 2.6 (2019), pp. 252–262. ISSN: 25201131. DOI: 10.1038/s41928-019-0258-6. URL: http://dx.doi.org/10.1038/s41928-019-0258-6.

[2] Syed Aziz Shah and Francesco Fioranelli. "RF Sensing Technologies for Assisted Daily Living in Healthcare: A Comprehensive Review". In: *IEEE Aerospace and Electronic Systems Magazine* 34.11 (2019), pp. 26–44. ISSN: 1557959X. DOI: 10.1109/MAES.2019.2933971.

[3] Adeel Ahmad et al. "Vital signs monitoring of multiple people using a FMCW millimeter-wave sensor". In: *2018 IEEE Radar Conference, RadarConf 2018* 4 (2018), pp. 1450–1455. DOI: 10.1109/RADAR.2018.8378778.

[4] C. G. Caro and J. A. Bloice. "Contactless Apnœa Detector Based on Radar". In: *The Lancet* 298.7731 (1971), pp. 959–961. ISSN: 01406736. DOI: 10.1016/S0140-6736(71)90274-1.

[5] Mari Zakrzewski, Harri Raittinen, and Jukka Vanhala. "Comparison of center estimation algorithms for heart and respiration monitoring with microwave doppler radar". In: *IEEE Sensors Journal* 12.3 (2012), pp. 627–634. ISSN: 1530437X. DOI: 10.1109/JSEN.2011.2119299.

[6] Lorenzo Scalise. "Non Contact Heart Monitoring". In: *Advances in Electrocardiograms - Methods and Analysis* (2012). DOI: 10.5772/22937.

[7] Changzhi Li and Jenshan Lin. "Complex signal demodulation and random body movement cancellation techniques for non-contact vital sign detection". In: *IEEE MTT-S International Microwave Symposium Digest* July (2008), pp. 567–570. ISSN: 0149645X. DOI: 10.1109/MWSYM.2008.4633229.

[8] Yiting Lu. "M . Sc . Thesis Development of Data Processing Algorithms for UWB Radar-based Long-Term Health Monitoring". In: (2019).

[9] Byung Kwon Park, Olga Boric-Lubecke, and Victor M. Lubecke. "Arctangent demodulation with DC offset compensation in quadrature Doppler radar receiver systems". In: *IEEE Transactions on Microwave Theory and Techniques* 55.5 (2007), pp. 1073–1078. ISSN: 00189480. DOI: 10.1109/TMTT.2007.895653.

[10] Ping Hsun Wu et al. "Phase- and self-injection-locked radar for detecting vital signs with efficient elimination of DC offsets and null points". In: *IEEE Transactions on Microwave Theory and Techniques* 61.1 (2013), pp. 685–695. ISSN: 00189480. DOI: 10.1109/TMTT.2012.2228222.

[11] Ashikur Rahman et al. "Doppler Radar Techniques for Accurate Respiration Characterization and Subject Identification". In: *IEEE Journal on Emerging and Selected Topics in Circuits and Systems* 8.2 (2018), pp. 350–359. ISSN: 21563357. DOI: 10.1109/JETCAS.2018.2818181.

[12] Isar Mostafanezhad et al. "Application of empirical mode decomposition in removing fidgeting interference in doppler radar life signs monitoring devices". In: *Proceedings of the 31st Annual International Conference of the IEEE Engineering in Medicine and Biology Society: Engineering the Future of Biomedicine, EMBC 2009* (2009), pp. 340–343. DOI: 10.1109/IEMBS.2009.5333206.

[13] Qin Zhou et al. "Detection of multiple heartbeats using Doppler radar". In: *ICASSP, IEEE International Conference on Acoustics, Speech and Signal Processing - Proceedings* 2 (2006), pp. 1160–1163. ISSN: 15206149. DOI: 10.1109/icassp.2006.1660554.

[14] Xiaolin Liang et al. "Ultra-Wideband Impulse Radar Through-Wall Detection of Vital Signs". In: *Scientific Reports* 8.1 (2018), pp. 1–21. ISSN: 20452322. DOI: 10.1038/s41598-018-31669-y. URL: http://dx.doi.org/10.1038/s41598-018-31669-y.

[15] Changzhi Li et al. "A review on recent advances in doppler radar sensors for non-contact healthcare monitoring". In: *IEEE Transactions on Microwave Theory and Techniques* 61.5 (2013), pp. 2046–2060. ISSN: 00189480. DOI: 10.1109/TMTT.2013.2256924.

[16] Guochao Wang et al. "A hybrid FMCW-interferometry radar for indoor precise positioning and versatile life activity monitoring". In: *IEEE Transactions on Microwave Theory and Techniques* 62.11 (2014), pp. 2812–2822. ISSN: 00189480. DOI: 10.1109/TMTT.2014.2358572.

[17] Marco Mercuri et al. "A Direct Phase-Tracking Doppler Radar Using Wavelet Independent Component Analysis for Non-Contact Respiratory and Heart Rate Monitoring". In: *IEEE Transactions on Biomedical Circuits and Systems* 12.3 (2018), pp. 632–643. ISSN: 19324545. DOI: 10.1109/TBCAS.2018.2813013.

[18] Iwaki Akiyama et al. "I -". In: September (2007), pp. 0–5.

[19] Yuan Liu et al. "Human respiration localization method using UWB linear antenna array". In: *Journal of Sensors* 2015 (2015). ISSN: 16877268. DOI: 10.1155/2015/601926.

[20] Tian Jin, Jun Lou, and Zhimin Zhou. "Extraction of landmine features using a forward-looking ground-penetrating radar with MIMO array". In: *IEEE Transactions on Geoscience and Remote Sensing* 50.10 PART2 (2012), pp. 4135–4144. ISSN: 01962892. DOI: 10.1109/TGRS.2012.2188803.

[21] Fulai Liang et al. "Detection of multiple stationary humans using UWB MIMO radar". In: *Sensors (Switzerland)* 16.11 (2016). ISSN: 14248220. DOI: 10.3390/s16111922.

[22] Siying Wang et al. "3D localization and vital sign detection of human subjects with a 120 GHz MIMO radar". In: *Proceedings International Radar Symposium* 2019-June (2019), pp. 1–6. ISSN: 21555753. DOI: 10.23919/IRS.2019.8768192.

[23] Raj Mittra and J. N. Bringuier. "A technique for solving multiscale problems in CEM utilizing dipole moments and macro basis functions". In: *EuCAP 2010 - The 4th European Conference on Antennas and Propagation* (2010), pp. 2–4.

[24] Michael Schoor and Bin Yang. "High-resolution angle estimation for an automotive FMCW radar sensor". In: *Proceedings International Radar Symposium* 2007-Janua (2007). ISSN: 21555753.

[25] Daegun Oh and Jong Hun Lee. "Low-Complexity Range-Azimuth FMCW Radar Sensor Using Joint Angle and Delay Estimation Without SVD and EVD". In: *IEEE Sensors Journal* 15.9 (2015), pp. 4799–4811. ISSN: 1530437X. DOI: 10.1109/JSEN.2015.2428814.

[26] Guochao Wang et al. "Linear-Frequency-Modulated Continuous-Wave Radar for Vital-Sign Monitoring". In: (), pp. 37–39.